J. Appl. Comput. Mech., 11(2) (2025) 303-326
DOI: 10.22055/jacm.2024.46291.4494

ISSN: 2383-4536
jacm.scu.ac.ir

Shahid Chamran University of Ahvaz

Journal of Applied and Computational Mechanics

Research Paper

Experimental Study on the Effect of Micro Concentrations of Hybrid Nanofluids through Microchannel Heat Sinks

Mohamed Salah Elsherbiny[1,2], Moustafa Ali[2], Moatsem Shahin[3], Mahmoud El-Kady[2]

[1] Renewable Energy Department, British University in Egypt, Cairo, Egypt

[2] Mechanical Engineering Department, Al-Azhar University, Nasr City, Cairo, Egypt

[3] Mechanical Engineering Department, Badr University in Cairo, Cairo, Egypt

Received March 05 2024; Revised July 17 2024; Accepted for publication July 16 2024.
Corresponding author: M.S. Elsherbiny (mohamed.salahelden@bue.edu.eg)

Abstract. The current study examines the convective heat transfer coefficient experimentally. It assesses the performance of Al_2O_3, CuO, ZnO, and Ag/ distilled water nanofluids up to a tetra level of hybridization utilized in microprocessor cooling systems equipped with MCHS. An equal ratio of 50%, 33.3%, and 25% for di-, tri-, and tetra-nanofluids, respectively, with a focus on micro-volume fraction 0.025% and comparing it with 0.05%. Operating conditions were as follows: heat loading from 136.4 up to 196.4 watts; and flow rate from 0.35 up to 0.5 LPM. The findings showed that all types of mono nanofluids showed an increase in Nu and HTC enhancement levels by increasing concentration from 0.025% to 0.05%, while HYNF reacted the opposite, even lower than the base fluid values. The reasons behind such findings might be due to the nanoparticle agglomeration effect. The maximum PEC was 1.845 at the highest heat flux and flow velocity by Al_2O_3-ZnO-Ag, while the minimum PEC was 0.847 at the highest heat flux and lowest velocity by CuO-ZnO-Ag, which is lower than unity. ZnO, Al_2O_3-CuO-ZnO, and CuO-ZnO-Ag only showed a PEC lower than unity; however, not in all operating conditions. Despite their differences in magnitude at 0.025%, all nanofluids showed an enhancement in terms of Nu and HTC ratios.

Keywords: Hybrid nanofluids, Tetra hybridization, Microchannel heat sinks, Microprocessor cooling systems, Micro-concentrations.

1. Introduction

Nanofluids and hybrid nanofluids, along with microchannel heat sinks, represent a cutting-edge trend in enhancing heat transfer for cooling high-heat flux devices, especially within constrained areas. Those approaches are particularly advantageous when dealing with devices that generate high heat loads in confined areas, like microprocessors, where traditional cooling methods may be insufficient. The relentless march towards the miniaturization of electronic devices and components has brought about significant challenges in the highly dynamic field of modern industrial applications such as micro-electro-mechanical systems (MEMS) and high-energy density electronic modules, especially in the area of thermal management. As these devices get smaller and more powerful, the increasing power density will eventually lead to higher temperatures and, consequently, system failure, which can account for around 55% of electronic component failures [1]. Microchannel heat sinks could tackle these thermal challenges because they maximize heat dissipation by taking advantage of miniaturization, as first reported by Tuckerman and Pease [2]. A significant improvement in thermal efficiency can be obtained with microchannel heat sinks, which are defined by finely crafted networks of tiny channels inside the cooling system, especially when utilizing nanofluids. When size, weight, and thermal considerations come together, the integration of microchannels becomes relevant, which not only optimizes the surface area to volume ratio but also deftly handles spatial constraints. Additionally, Khan et al. [3] defined and categorized channels in a review into mini channels and microchannels, with mini channels having a size range from 200 micrometers to 3 millimeters and microchannels having a size range from 10 micrometers to 200 micrometers. This method advances the thermal performance of small systems while meeting the demands of modern electronics, which place a premium on efficiency and compactness. The evolution of cooling in such systems started with natural convection, then forced air cooling with a metal sink, and finally liquid cooling for much higher power as high heat density affects chip performance just to keep up with Moore's law of increasing transistor density on a single chip and the ongoing demand for more efficient cooling systems [4].

Enhancing the advancements in microchannel technology, the use of nanofluids is a novel way to leverage and improve heat transfer characteristics. A new approach to thermal management is offered by nanofluids, which are colloidal suspensions of

Published online: July 28 2024

nanoparticles within base fluids, and it was first proposed by Choi and Eastman [5]. The thermal conductivity of the nanoparticles, which are frequently metal- or metal oxide-based, raises the fluid's overall heat transfer properties. Thus, heat dissipation is enhanced, making nanofluids an attractive option for cooling miniature systems in situations where conventional fluids might not be sufficient. Moreover, nanofluids' tunability is what gives them their versatility. By regulating the concentration and dispersion of nanoparticles, the thermal characteristics of a fluid can be enhanced to suit the unique needs of a variety of applications. Hybrid nanofluids, which combine various nanoparticles into a single fluid medium, are even more innovative than before, as hybrid or composite nanofluids are thought of as an extension of research into single nanofluids, which can be accomplished through the dispersion of two or more different nanoparticles in liquid base fluid. By utilizing the combined benefits of various nanoparticles, this method produces a hybrid colloidal that can exhibit higher thermal conductivity than single-component nanofluids. A sophisticated approach to heat management is made possible by nanofluids, which provide improved performance and flexibility tailored to the complex requirements of diverse industrial applications. However, heat transfer enhancement mechanisms proposed, like Brownian motion, liquid layering, and nanoparticle aggregation, failed to project a complete map and left a lot of gaps that needed to be filled. Hybrid nanofluids are the key to a deep understanding of nanotechnology and how they enhance heat transfer capabilities.

These miniature cooling technologies hold great promise for extending the lifespan and reliability of electronic parts, avoiding malfunctions brought on by overheating, and guaranteeing steady operation. Effective thermal management is crucial for success in industries such as advanced computing, telecommunications, automotive, and renewables, where processing power is always increasing. Finally, employing nanofluids and microchannel heat sinks not only might help to solve the thermal issues that miniaturization presents today but also lays the groundwork for the next generation of cooling technologies. In the literature, there are two methods for preparing nanofluids from nanoparticles: the one-step method and the two-step method. The two-step method is more frequently used in the literature due to its advantages and flexibility over the one-step method. Many researchers have used the two-step method for preparing hybrid nanofluids, such as Suresh et al. [6] for preparing di-hybrid nanofluids and Ramadan et al. [7] for preparing tri-hybrid nanofluids. Additionally, Khan et al. [3] reviewed the use of nanofluids in micro- and mini-channels, and preparation using the two-step method is preferable due to the ability to make more sophisticated and stable nanofluids than the one-step method. The stability of nanofluids is one of the main issues with this new technology. Sonication, magnetic stirrers, and surfactants were a few of the technologies examined that were recommended in the literature to increase stability. Additionally, there are four common methods for evaluating stability. According to Zeta potential, centrifugation, the sedimentation photo method, electron microscopy, and other methods, however, the photographic method for tracking the sedimentation of nanoparticles was the most commonly used in the literature. There hasn't been much experimentation done on hybrid nanofluids, and there hasn't been any established correlation between thermophysical properties and heat transfer characteristics [8]. In addition, many researchers performed different techniques to enhance stability. SDS was agreed to be a good dispersing agent used by many researchers, as Vinoth and Sachuthananthan [9] used it for preparing mono- and hybrid nanofluids.

A precise estimation of nanofluid's thermophysical properties is a requirement for thermal liquid convective problems, especially as those properties in the case of nanofluids and hybrid nanofluids are manipulated as tested parameters change, such as nanoparticle concentration, particle size, hybridization ratio, and fluid flow temperature or flow velocity. Thus, investigators started to develop models and equations for estimating those properties, such as thermal conductivity, density, dynamic viscosity, and heat capacity. Attempts were undertaken with two main approaches: a temperature-dependent approach and a temperature-independent approach. The oldest and most commonly used model is the Maxwell model; moreover, Nitiapiruk et al. [10] investigated three different models while studying convective heat transfer in microchannel heat sinks using mono nanofluid and found that the difference among the Nusselt numbers predicted by the various models is about 2%, which is not significant. In the wide domain of convective heat transfer within microchannels utilizing nanofluids, a group of researchers employed them experimentally [9, 11-13], while another group investigated them numerically using different types of techniques and algorithms [14-18]. Moreover, it is noticed that the number of experimental studies is much fewer than the numerical ones; however, the vitality of the experimental investigations for understanding the enhancement mechanism and phenomenon behavior for highlighting the reasons behind enhancement or diminished values of heat transfer coefficient and hydrothermal performance. In the pursuit of understanding, investigators delve deep into the examination of various geometric parameters to reveal the inner workings of microchannel heat transfer. Jajja et al. [19] investigated the effect of fin spacing on mini channel heat sinks from 0.2 to 1.5 mm and concluded that the increase in flow rate and decreasing fin spacing decreased the base temperature and thermal resistance. The exploration spans dimensions such as size [19], cross-sectional configurations [20], and single and double-layered channels [15], where each parameter contributes to the grand knowledge of the thermofluidic behavior of those systems. Furthermore, it expands to include linear and nonlinear arrays [17, 21] and studies the relationships between spatial arrangements and their profound impact. However, that approach to geometrical changes has its inherent limitations, besides the lack of investigations into such modifications and their impact employing hybrid nanofluids and higher levels of hybridized nanofluids.

From the point of view of nanofluids and their parameters, investigators called single-type nanofluids mono-nanofluids and studied them through a mini-channel heat sink [20, 22] or a micro-channel heat sink [15, 23]. For mini channel heat sinks, El-Khouly, El Bouz, and Sultan [22] studied experimentally and numerically CuO/Water at a concentration range from 0.5% to 5% per volume and found a maximum enhancement in thermal conductance of 8.1% and maximum overall thermal-hydraulic performance at the highest tested concentration, while Khoshvaght-Aliabadi et al. [20] investigated numerically Al_2O_3/Water at a concentration range from 0% to 4% and various heat sink cross-section areas (elliptic, half-circular, rectangular, triangular, and square), and the results showed an optimum value at square and volume fraction of 1% with an average enhancement of 1.04 to 1.51. While, for microchannel heat sinks, Elbadawy and Fayed [15] studied Al_2O_3/water numerically at Reynolds number range from 200 to 1500 and concentration from 1% to 5% per volume, and the study revealed that maximum reduction of surface temperature at maximum concentration was 33.5% and maximum enhancement heat transfer coefficient for nanofluids over pure base fluid was 13.12%, while, Azizi et al. [23] studied experimentally Cu/water nanofluid at a range of concentrations from 0.05 to 0.3 percent per weight and results showed higher flow rates leads to smaller temperature drop and states that optimum value of flow rate is vital and maximum Nusselt enhancement was at the highest concentration up to 1.3.

Hybrid nanofluid is defined as using more than one particle nature in generating nanofluids, and recently, it has been one of the most promising research trends investigated in many fields, especially cooling electronic devices. Researchers investigated hybrid nanofluids differently; some tried mono-nanofluids versus their hybridizations, and others investigated using different types of hybrid nanofluids to highlight which of them performed better thermally, while a few others investigated higher levels of hybridization. Some researchers focused on graphene-based hybrid nanofluids [24, 25] in mini- and microchannels. Kumar, Sarkar, and Yan [24] investigated hybrid reduced graphene oxide with zinc oxide at a constant concertation of 0.01% per volume and an aspect ratio of channel from 2.5 to 5, and the results obtained showed that reduction in aspect ratio enhances heat transfer coefficient by 47.2% at higher flow rates and heat transfer increased by 17.41% with the increasing heat flux, while performance evaluation criteria show a trend of decrease, increase, then decrease with the flow rate. Additionally, Bahiraei et al. [25] investigated hybrid graphene-silver nanofluid, and the average convective heat transfer coefficient was enhanced by increasing the concentration from 0 to 0.1% and recorded 17% maximum enhancement. From a hybrid nanofluid perspective, researchers have recently started to investigate its hydrothermal performance in numerous applications; however, it does not always come with positive feedback. Moreover, very few researchers have investigated its hybridization effect and higher levels of hybridization than di-hybrid nanofluids. Following some studies that used hybrid nanofluids, Sarvar-Ardeh et al. [26] studied two different types of hybrid nanofluids by hybridizing Al_2O_3 with Cu and SiO_2 with water as the base fluid to create two hybrid nanofluids numerically. The heat sink used in that study was a double-layered microchannel heat sink with different volumetric macro concentrations from 1% to 5% per volume, and results showed that the base surface temperature is decreased by using both nanofluids compared to the base fluid, while Al_2O_3-SiO_2/water showed a better cooling capacity, lower thermal resistance, and better Nusselt numbers compared to the other type of hybrid nanofluids. Generally, increasing the volumetric concentration of nanofluids reduces thermal resistance and raises the pressure difference across the heat sink. While Sriharan et al. [12] investigated experimentally three different types of di hybrid nanofluids, Al_2O_3-SiO_2/water, Al_2O_3-CuO/water, and CuO-SiO_2/water, at a hybridization ratio of 80:20, respectively, and a fixed macro concentration of 0.3% per volume passing through a mini channel heat sink, and they reported that increasing the volume flow rate from 0.1 to 0.5 liters per minute promotes Brownian motion, leading to an enhancement in cooling values among all tested hybrid fluids, besides, highlighting that Al_2O_3-CuO/water nanofluid provides maximum enhancement in heat transfer coefficient, effectiveness, and Nusselt number by 54.5%, 42%, and 28.4%, respectively.

Another wave of studies approached hybridizing two types of mono-nanofluids and comparing the di-hybrid with their mono-nanofluid types. Experimentally, by studying mini-channel heat sinks, Kumar et al. and Ataei et al. [11, 13] investigated that approach. Kumar et al. [11] studied alumina, graphene, and alumina-graphene hybrid compositions at a micro-concentration of 0.01% per volume with water-base fluid and a low Reynolds number range from 80 to 450 and recorded an increment in convective heat transfer coefficient of 30.93% with graphene/water compared to water-based fluid, higher values than other blinds, including hybrid ones, and a 23.82% pressure drop. However, the Al_2O_3-Gr hybrid nanofluid delivers an optimum comparison factor, which means heat transfer coefficient to pressure drop ratio, along with a lower entropy generation rate among other investigated fluids. On the other hand, Ataei et al. [13] studied TiO_2/water, Al_2O_3/water, and Al_2O_3-TiO_2/water nanofluids at a macro-volume fraction of 0.5% and a higher Reynolds number range of 400 to 1000. The findings showed that convective heat transfer coefficient maximum enhancement was up to 16.97% at the lowest Reynolds number tested, and wall temperature was reduced up to 5 °C using Al_2O_3-TiO_2/water di- hybrid nanofluid, which recorded a higher value of enhancement than mono-nanofluids. Investigating higher levels of hybrid nanofluids is rarer in the literature, especially when utilizing microchannel heat sinks. As far as our knowledge from an experimental perspective, Ramadan et al. [7] investigated tri-hybrid nanofluid, not in micro or mini channel heat sinks but in a conventional car radiator, by investigating Al_2O_3-TiO_2-SiO_2 tri-hybrid nanofluid in water-ethylene glycol 60:40 percent as a base fluid. The nanofluid parameters were as follows: a constant hybridization ratio of nanoparticles of 1/3:1/3:1/3 and a variable nanoparticle concentration of 0.05% to 0.3% per volume. The study showed a maximum enhancement from the coolant side of 39.7% at the highest tested concentration of tri-hybrid nanofluid. Furthermore, Souby et al. and Zahan et al. [27, 28] investigated tri-hybrid nanofluids using numerical methods; however, Zahan et al. [28] investigated them through a conventional convergent-divergent nozzle numerically using computational fluid dynamics CFD, using Navier-Stokes equations and energy equations, and solved them by finite element method FEM. That study used Cu-Ag-Zn nanoparticles submerged in different base fluids: water, ethylene glycol, and a water-ethylene glycol mixture with 50:50 and 60:40 percent, respectively, while hybridization ratios were as follows: 0:1/2:1/2, 1/2:0:1/2, 1/6:1/6:2/3, 1/6:2/3:1/6, 2/3:1/6:1/6, and 1/3:1/3:1/3, respectively. The results showed that ethylene glycol base fluid with a 1/3:1/3:1/3 hybridization ratio showed the maximum increase in Nusselt number by 10.30% as concentration increased from 0.01 to 4%, while the 1/6:2/3:1/6 hybridization ratio showed a relatively higher heat transfer coefficient compared to other combinations. On the other hand, Souby et al. [27] investigated MgO-TiO_2 and CuO-MgO-TiO_2 hybrid nanofluids through a microchannel heat sink in a macro-concentration range of 0.1 to 0.5% per volume, and it was shown that higher values of the convective heat transfer coefficient, pressure drop, and frictional entropy generation rate are obtained when using hybrid nanofluids with higher values of Reynolds number and volumetric concentrations.

Furthermore, it is worth mentioning that encapsulated phase change materials (PCM), magnetic nanofluids, and porous medium heat sinks are emerging as promising avenues to enhance heat transfer efficiency alongside nanofluids. PCM, with their ability to store and release large amounts of latent heat during phase transitions, offers efficient thermal management in various applications; thus, researchers started to enrich that approach from different perspectives, whether investigating it experimentally [29] or numerically [30]. Moreover, magnetic nanofluids, infused with magnetic nanoparticles, exhibit tunable thermal conductivity under the influence of external magnetic fields, enabling precise control over heat transfer rates or increasing heat transfer rates by enhancing flow dynamics and better entity mixing; thus, many investigators studied their effects utilizing nanofluids [31] and hybrid nanofluids [32], whether by experimental methods [31] or numerical methods [32]. Further, porous medium heat sinks despite the fabrication barrier utilize the high surface area of porous structures to enhance convective heat transfer, making them effective in dissipating heat from electronic devices and other systems; thus, researchers studied their effect on different heat transfer modes employing nanofluids in either free convection [33], mixed convection [34] or forced convection [35] applications. These innovative approaches were recently proposed as well towards addressing heat transfer challenges in diverse industries.

After a careful review, it is obvious that manipulating nanoparticle volume fractions for nanofluids and hybrid nanofluids at the micro-concentration level is very limited compared to macro-concentrations, and one of the reasons is that most literature found that a higher value of enhancement for heat transfer coefficient can be obtained by using a higher value of concentration; however, that might be different in the case of using hybrid nanofluids. As shown in Table 1, a review of the literature from a concentration-level perspective for nanofluids and hybrid nanofluids at macro and micro concentrations, mostly for microchannel heat sinks, with their findings listed, One of the findings from that review was that besides nanofluid parameters like concentration, particle size, particle shape, and hybridization, hydrothermal operating parameters like flow velocity, Reynolds number, and the range of heat load applied to the system also affect the thermal performance of nanofluids and hybrid nanofluids. Furthermore, higher levels of macro-concentration have not always shown an enhancement in heat transfer capabilities; besides, micro-concentration mostly uses graphene-based nanofluids or hybrid nanofluids; and finally, nanofluids showed enhancement and diminished values for both levels of concentration.

Table 1. Review of using different levels of concentration of nanofluid and hybrid nanofluid in MCHS.

Concentration level	Authors	Nanofluid and heat sink type	Concentration tested	Findings
Macro	Farsad et al. [36]	- Al_2O_3, CuO and Cu/water - MCHS	0, 2, 4, 6, 8% vol.	• Increasing concentrations reduce the wall temperature of the heat sink • Increasing concentration from 2% per volume up to 8% reduces the maximum recorded wall temperature to about 1% for Al_2O_3
	Krishna et al. [37]	- MWCNT-CuO/water and CuO/water - MCHS	0.5, 1, 2,3% vol.	• While increasing the concentration up to 3% per volume, hybrid nanofluid showed better-enhanced values over mono nanofluid
	Mohammed et al. [38]	- Al_2O_3/water - MCHS	1, 2.5, 5% vol.	• At the lower heat flux range, nanofluids had no effect over pure water • At high heat flux ranges, increasing concertation of nanoparticles enhanced the heat transfer coefficient. However, 5% could not enhance the heat transfer
	Sarvar-Ardeh et al. [26]	- Al_2O_3-Cu/water and Al_2O_3-SiO_2/water - MCHS	1, 3, and 5% vol.	• Al_2O_3-SiO_2 hybrid nanofluid showed better cooling among the tested ones • Increasing concentrations of the hybrid nanofluids reduced their thermal resistance. However, it showed a reduction trend with increasing Re numbers
	Hung et al. [39]	- Al_2O_3, CuO, TiO_2, Diamond, Cu and Ag - Ethylene glycol, Engine oil and water - MCHS	0.5, 1, 2, and 5% vol.	• Increasing concentrations of nanoparticles have not always had a positive effect on enhancing heat transfer coefficients • Al_2O_3/water showed the best performance among all nanofluids, and its optimum recorded concentration was 2%
	Souby et al. [27]	- MgO-TiO_2/water, CuO-MgO-TiO_2/water - MCHS	0.1-0.5% vol.	• Higher values of convective heat transfer coefficient and maximum reduction in total thermal resistance for the tested di and tri hybrid nanofluids were recorded at the highest values of concentration and Re number
	Al-Rashed et al. [16]	- CuO/ water-CMC 0.5% wt. - MCHS	0.5,1,1.5,3 vol.	• At the studied concentration and Re number range, the maximum heat transfer coefficient was recorded for the highest values of those parameters
Micro	Bahiraei et al. [40]	- Gr-Ag/water - MCHS	0.02, 0.06 and 0.1% vol.	• The surface temperature and thermal resistance were reduced, and cooling uniformity improved for both heat sinks by increasing either velocity or particle concentration
	Samal et al. [18]	- Gr-Ag/water - Recharging microchannel (RMC)	0, 0.02, 0.06 and 0.1% vol.	• HYNF with a higher volumetric concentration and higher velocity shows better cooling performance by reducing the maximum substrate temperature and thereby increasing temperature uniformity
	Singh et al. [41]	- CNT - MCHS	0.001 to 0.005% vol.	• A comparison has been done with water, and the heat transfer coefficient increased in the case of CNT nanofluids with a higher concentration as compared to water with an upstream triangular shape
	Kumar et al. [42]	- Al_2O_3-TiO_2 - Mini channel heat sink	0.1% vol.	• Both numerical and experimental results reveal that the hybrid nanofluids yield no synergetic effect in heat transfer while mixing dissimilar nanoparticles of similar shape and size

Additionally, a review performed for many literature reviews focused on mini and microchannel heat sinks employing nanofluids and hybrid nanofluids in microcooling systems [3, 42-44]. The conclusions were that increasing macro-concentrations of hybrid nanofluids enhances heat transfer up to a certain limit; after that, there is no effect; however, micro-concentrations were recommended for the many advantages when utilizing hybrid nanofluids; consequently, some hybrid nonfluids showed promising heat transfer capabilities and other hybrid nanofluids showed the opposite, even lower than base fluid values. Along with a lack of scientific knowledge of the process accountable for property changes, the inadequate analysis of suspensions, and a reasonable proposal for the mechanism of enhancement and the phenomenon behind it, all lead to the need for considerable reasoning to be carried out using hybrid nanofluids because of the stability and production cost of nanofluids and the potential to provide answers over nanofluids. Despite the multitude of studies, a gap emerges within the literature, akin to an unexplored sector for studying intensively microchannel heat sinks while changing the different parameters of working nanofluids. That void pertains to a lack of comprehensive exploration into the dynamic interplay between changing nanofluid parameters like particle concentration and level of hybridization and their effects on the aforementioned geometric intricacies. Hybrid nanofluids hold the key to a deep understanding of how nanotechnology improves heat transfer capabilities, as literature results range from higher enhancement to depreciate effects. This highlights the potential discoveries and presents opportunities for future research to unveil the subtle interactions between nanofluid characteristics and microchannel heat transfer studies. Studying the manipulation of micro-concentrations on microchannels is very rare, especially when it comes to experimental contributions, which become even rarer, highlighting the novelty and what makes the current study unique. Finally, it is clear from the earlier studies that using microchannel heat sinks and hybrid nanofluids at higher levels of hybridization or different hybridization ratios in research has exponentially increased interest, especially from an experimental perspective as it is still in its early stages.

So, the objective of this study is to present an experimental investigation of using a hybrid nanofluid as a coolant flowing through a copper microchannel heat sink on a simulated microcooling system rig used as a microprocessor cooling unit. From mono to tetra hybrid nanofluids for Al_2O_3, CuO, ZnO, and Ag nanoparticle identities with distilled water as a base fluid was prepared, while the hybridization level was up to tetra level with equal hybridization ratios of 50%, 33.3%, and 25% for di, tri, and tetra nanofluids, respectively. The study focused on testing 0.025% per volumetric micro-concentration and comparing it with a higher micro-concentration level of 0.05% per volume. The heat transfer characteristics like heat transfer coefficient ratio, Nusselt number ratio, and performance evaluation criteria were evaluated for the following operating conditions: various heat loading ranges (136.4, 158.19, 180, and 196.4 Watts) and flow rate ranges (0.35, 0.4, 0.45, and 0.5 LPM) to study intensively how various parameters could affect cooling system performance and to reveal how hybrid nanofluids at higher levels of hybridization could react with microchannel heat sinks in terms of overall hydrothermal performance.

2. Experimental Setup

2.1. Experimental test rig and test specimen and microchannel heat sink

The experimental test rig was designed to simulate a microprocessor liquid cooling system running under different computing conditions, performed by controlled heat loads aligned with a controlled coolant volumetric flow rate, and fitted with the necessary measurement devices and instruments. For simulating a convective liquid cooling system, an I9-type microprocessor is an intricate and multifaceted setup, visually represented through a detailed schematic figure as shown in Fig. 1. for providing readers with a comprehensive overview of the system's layout, aiding in a nuanced understanding of its components and functionality.

Complementing that detailed figure, a photographic image as shown in Fig. 2. depicts the overall layout of the experimental setup, showing the front and back views and highlighting the names of each component. This inclusive illustration captures the interconnected components, including the microchannel heat sink, air cooler with a fan, liquid pump, expansion tank, and an intricate network of sensors. The liquid DC pump aims to circulate the coolant through the system, in addition to supporting the expansion tank with a fluid filling point. Additionally, the system is supported by an electronic flowmeter (YF-S401 Sensor) to measure the flow rate necessary for the study beside two mechanical ball valves, the first for controlling and manipulating the flow rate to reach the desired values for the investigation, while the second one serves as a drainage point at the lowest point in the system. Furthermore, the figure highlights the analog pressure sensors G1/4 and temperature sensors (calibrated thermocouples of the K-type), measuring both inlet and exit fluid pressure and temperature, for understanding the fluid dynamics and heat transfer within the system. This schematic provides a general perspective on the system's layout and the interactions between its various elements. Moreover, the experimental system incorporates a data acquisition card (DAQ) to gather precise measurements from sensors placed throughout the setup, ensuring detailed data collection for further analysis of the thermal dynamics.

One key element highlighted in a dedicated figure is the copper microchannel heat sink, a critical component to ensure efficient microprocessor cooling. This detailed illustration includes specific dimensions of the microchannels as shown in Fig. 3, offering a visual representation and a schematic diagram supported with dimension names for further calculations. The microchannel's width is 117 micrometers, so to calculate the hydraulic diameter, surface area, and cross-sectional area, the microchannel's variables must be precisely defined. Another pivotal aspect showcased in a separate figure, as shown in Fig. 4, is the test specimen that simulates an I9-type microprocessor, represented by a copper rod. This figure provides a detailed view of the placement of thermocouples along the copper rod, emphasizing the points where temperature measurements are obtained. Additionally, the 400-watt cylindrical heater used around the test specimen is controlled by an electric voltage regulator, which plays a role in simulating various microprocessor loads. Furthermore, to ensure clarity regarding the setup's thermal insulation, the copper rod is insulated with glass wool to prevent any heat loss to the surroundings.

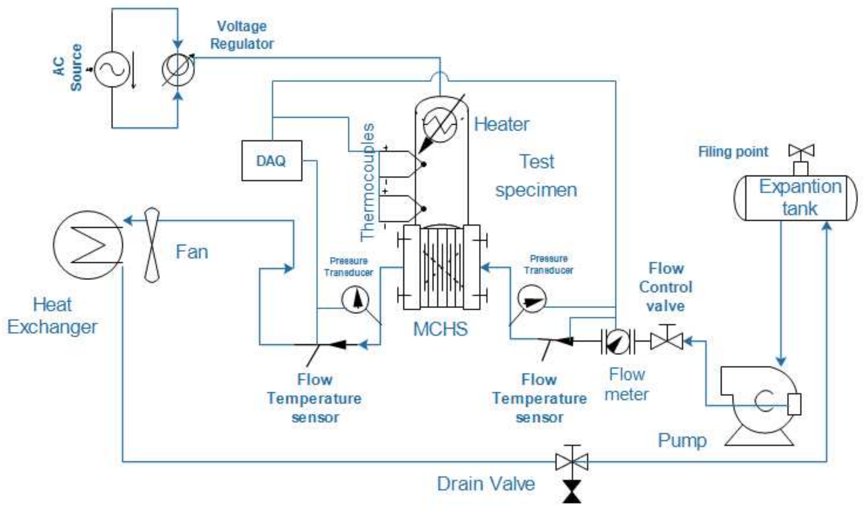

Fig. 1. Schematic diagrams for test rig showing all components.

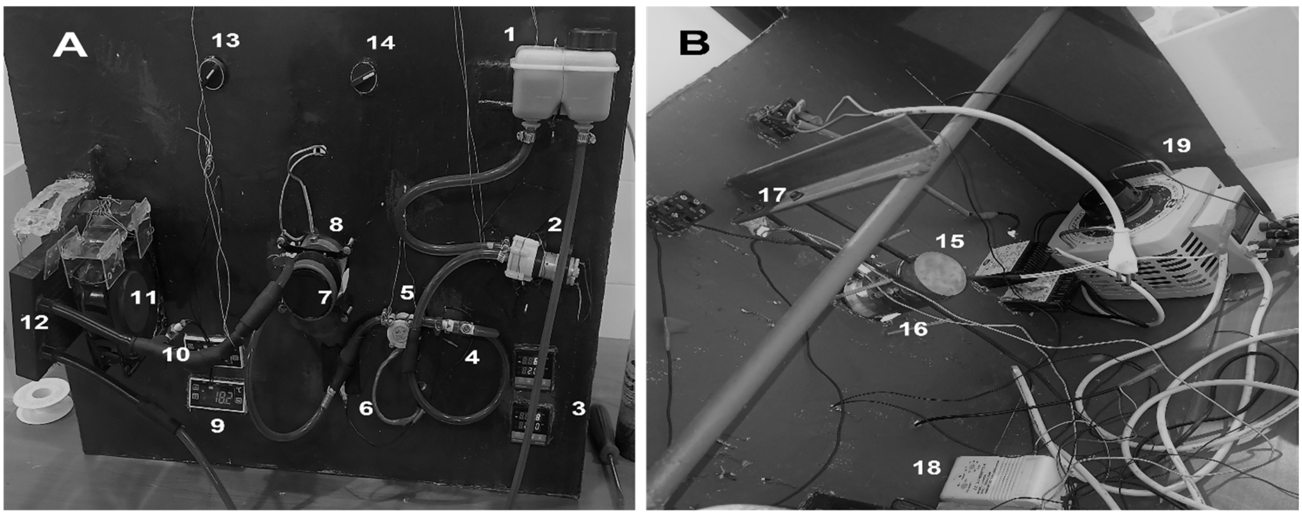

Fig. 2. Photographic image of the test rig utilized to simulate the microprocessor liquid cooling system. (a) Test rig front view, (b) Test rig back view, (1) Expansion tank and filling point, (2) Circulating pump, (3) Specimen temperature readout, (4) Flow control valve, (5) Flow rate sensor, (6) Coolant inlet temperature and pressure sensors, (7) Micro channel heat sink, (8) Specimen temperature sensors, (9) Coolant temperature readout, (10) Coolant outlet temperature and pressure sensors, (11) Fan, (12) Air heat exchanger, (13) Fan on-off switch, (14) Pump on-off switch, (15) Test specimen, (16) Circular electric heater, (17) Screw leveling and support of test specimen, (18) Pump power supply.

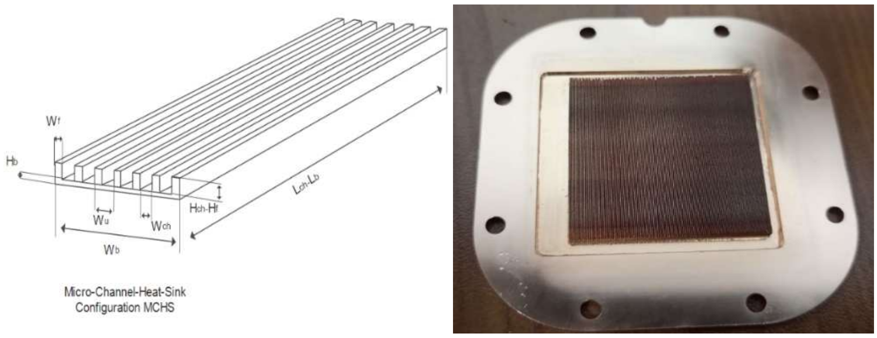

Fig. 3. The microchannel heat sink employed in the experiment was captured in photographic and schematic views.

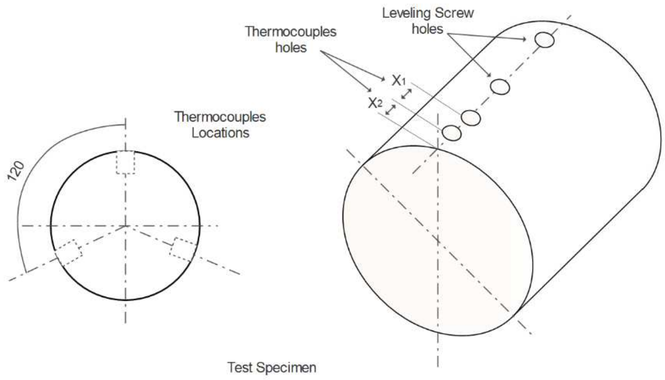

Fig. 4. Test specimen schematic diagram showing measurement spaces and angles.

The overall design is completed with the integration of temperature readers, providing real-time monitoring and feedback. These readers display temperatures, including fluid temperatures entering and exiting the microchannel, as well as two levels of temperature on the copper specimen. This multifaceted temperature monitoring approach ensures a detailed understanding of heat flux and surface temperature dynamics during experimental trials, in addition to approaching the steady-state point of the system. In summary, the combination of detailed schematic figures, such as the microchannel heat sink and a simulated microprocessor, and monitoring systems, including the DAQ and temperature readers, positions this experimental test rig as a research platform for in-depth research into convective liquid cooling systems for high-performance microprocessors. The test rig is supported by an air heat exchanger radiator and an AC fan used for cooling the coolant by air-forced convection. It is important to note that the microchannel heat sink and the system are an actual commercial system used for cooling microprocessors of the I9 generation Xigma Tek Aurora 120.

The test specimen has six holes distributed as shown in Fig. 4, each of the two holes has an angle difference of 120 degrees to ensure an efficient heat flux measurement through the test specimen, while there are two screw holes to support the rod to the structure of the test rig and to control the leveling of the specimen with the level of the MCHS, moreover, the distance between the two levels of thermocouples shown as x_1 and x_2 is 0.5 mm. Furthermore, six thermocouples of 0.5 mm wire diameters are installed and connected to the DAQ and the temperature readouts. Moreover, to prevent liquid leakage, Teflon coats were used. The specimen's top surface must be at the same horizontal level as the inner bottom surface of the MCHS to prevent heat dissipation, thus, both are connected to a thermal paste and isolated using glass wool. The close readings of the thermocouples (around 1° difference) in each level indicate the heat flux uniformity through the test specimen. The average reading in each plane is used in the heat flux calculations.

Furthermore, for further calculations, it is required to measure and calculate all geometric parameters and dimensions for the test specimen and microchannel heat sink. As for the test specimen, it is required to calculate the cross-sectional area by Eq. (1), while for the microchannel heat sink, it is required to calculate the value of the surface area of the microchannel heat sink as it is the convective heat transfer area by Eq. (2). Following that, all measured geometrical parameters related to microchannel are collected and represented as shown in Table 2:

$$A_{cr_{sp}} = \frac{\pi}{4} d_{sp}^2 \tag{1}$$

$$A_s = L_{ch} w_{ch} N_{ch} + L_f w_f N_f + 2 L_{ch} H_{ch} N_{ch} \tag{2}$$

where the subscriptions *cr* means cross-sectional, *ch* means channel, *f* means fins, *s* means the surface, and finally, *sp* means specimen.

Table 2. List of dimensions and values of the microchannel heat sink.

Name	Number of fins	Width of fin	Width of channel	Length of channel	Height of channel
Character	N_{ch}	w_f	w_{ch}	L_{ch}	H_{ch}
Value	159	58	117	0.028	0.008
Unit	-	μm	μm	m	m

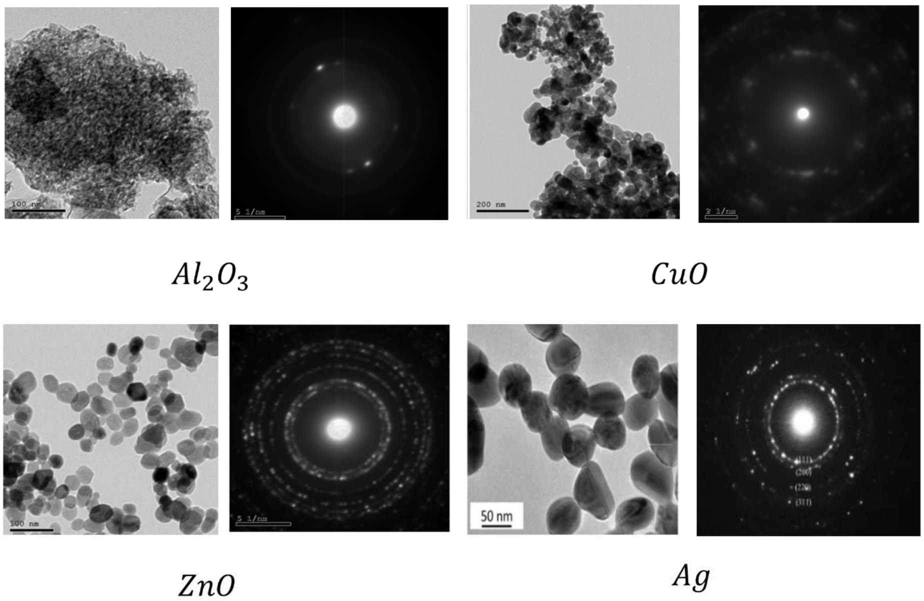

Fig. 5. The TEM image and SAED for Al_2O_3, CuO, ZnO, and Ag nanoparticles.

2.2. Nanofluid preparation and properties evaluation

The next step, after discussing and representing all details related to the microchannel heat sink and test specimen, is to discuss and represent the details related to the coolant fluid types. The base working fluid tested through the experiment was distilled water, and the nanoparticles' chosen identities were Al_2O_3, ZnO, CuO, and Ag for creating numerous nanofluid types. Nanoparticles tested through the investigation were purchased from Nanogate, a company located in Egypt, and supported with the characterizations and thermophysical properties data. A collective image showed transmission electron microscopy TEM and selected area electron diffraction SAED for all types of nanoparticles used as shown in Fig. 5 for creating nanofluids and hybrid nanofluids. Moreover, the basic properties and qualities like appearance, form, color, shape, and average particle size are also given by its datasheet. It's vital to have tabulated data for all the properties and characteristics of each entity using base fluid and nanoparticles, especially for thermophysical properties, as it is used for further experimental calculation. Besides, it is pivotal for analyzing the results and findings, as shown in Table 3.

Al_2O_3, ZnO, CuO, and Ag nanoparticles were used in the study for generating mono, di, tri, and tetra nanofluids. An important step for preparing nanofluids and hybrid nanofluids was to calculate precisely the mass required for each type of nanoparticle to achieve the correct overall volumetric concentration for each trail of nanofluids and hybrid nanofluids. So, by calculating the volumetric concentration of each nanoparticle identity in hybrid nanofluids based on the hybridization ratio required for each iteration, it was multiplied by the total volume of nanoparticles to calculate the specific amount of mass needed for each type to achieve that concentration using Eqs. (3) to (5):

$$\varphi_t = \sum_n \varphi_{np} \tag{3}$$

$$V_{np} = \varphi_{np} V_{bf} \tag{4}$$

$$m_{np} = V_{np} \rho_{np} \tag{5}$$

As the subscriptions t means total, bf means base fluid and np means nanoparticles.

Table 3. Thermophysical properties and characteristics of coolant entities, base fluid, and nanoparticles used supported by the manufacturer.

Property	Unit	Al_2O_3	CuO	ZnO	Ag	Water
Density	kg/m^3	3890	6315	5585	10500	997
Specific Heat	j/kg.k	880	540	495	235	4180
Thermal Conductivity	w/m.k	40	33	29	429	0.613
Viscosity	Pa.s	-	-	-	-	0.0010016
Particle Avg. Size (TEM)	nm	< 30	< 50	35±5	< 50	-
Particle Shape (TEM)	-	Spherical	Spherical	Spherical	Spherical	-
Particle Type	-	Metal oxide	Metal oxide	Metal oxide	Metal	-
Appearance (color)	-	White	Dark brown to black	White to yellow	Gray	-
Molecular Weight	g/mol	101.96	79.55	81.41	107.87	-
Bond Spacing	Å	1.76 and 1.97	1.95-1.96	2-2.01	2.88	-
Molecular Crystalline Structure	-	Corundum structure, triagonal shape	Square coplanar geometry	Hexagonal structure	Cubic structure	Tetrahedral geometry

Table 4. Hybridization ratio trials were implemented in the conducted experiment.

Hybridization level	Mono				Di						Tri				Tetra
Trails	1	2	3	4	5	6	7	8	9	10	11	12	13	14	15
Al_2O_3	100	0	0	0	50	50	50	0	0	0	0	33.3	33.3	33.3	25
ZnO	0	100	0	0	0	50	0	0	50	50	33.3	33.3	0	33.3	25
CuO	0	0	100	0	50	0	0	50	50	0	33.3	0	33.3	33.3	25
Ag	0	0	0	100	0	0	50	50	0	50	33.3	33.3	33.3	0	25

At a constant micro-concentration of 0.025% per volume, different mixture ratios are prepared, covering all possible trials that could be done using four types of nanoparticles up to the tetra level of hybridization and that generated four types of mono nanofluids, six types of di nanofluids, four types of tri-nanofluids, and one tetra nanofluid using an equal hybridization percentage at each level. As shown in Table 4, the conducted trials are illustrated with their hybridization ratios. In this investigation, nanofluids were prepared using a two-step method by using a magnetic stirrer for 2 hours followed by 1 hour of sonication time to establish a uniform, stable dispersion supported with sodium dodecyl sulfate SDS as a dispersant at a concentration of 0.05% per volume to ensure high mixture stability. For stability check, the resultant nanofluid is observed, and mixtures start sedimentation 10 days on average, as it was noticed that as the hybridization level increases, sedimentation occurs relatively earlier. Furthermore, the approach used in the current study for evaluating the thermophysical properties of nanofluids and hybrid nanofluids was a temperature-independent approach. The thermophysical characteristics of the nanofluids like density, specific heat capacity, thermal conductivity, and dynamic viscosity were determined using the following classic models Eqs. (6) to (9), respectively [9, 15, 22, 23, 38, 42, 45]:

$$\rho_{nf} = (1-\varphi_t)\rho_{bf} + \sum\nolimits_n \varphi_{np}\rho_{np} \tag{6}$$

$$c_{p_{nf}} = \frac{(1-\varphi_t)\rho_{bf}c_{p_{bf}} + \sum\nolimits_n \varphi_{np}\rho_{np}c_{np}}{\rho_{nf}} \tag{7}$$

$$\frac{k_{nf}}{k_{bf}} = \frac{(1/\varphi_t)\sum\nolimits_n \varphi_{np}k_{np} + 2k_{bf} + 2\sum\nolimits_n \varphi_{np}k_{np} - 2\varphi_t k_{bf}}{(1/\varphi_t)\sum\nolimits_n \varphi_{np}k_{np} + 2k_{bf} + 2\sum\nolimits_n \varphi_{np}k_{np} + 2\varphi_t k_{bf}} \tag{8}$$

$$\mu_{nf} = \left(1 + 2.5\varphi_t + 6.5\varphi_t^2\right)\mu_{bf} \tag{9}$$

where *nf* means nanofluid, *bf* means base fluid, *np* means nanoparticles, *t* means total and *n* means a number representing the level of hybridization.

2.3. Experimental procedures, data reduction, and error analysis

The experimental procedures start with a flushing system using hot distilled water, and this step is repeated carefully after each coolant type run to remove any contaminants and ensure that the working nanofluid is free of any contaminants from the previous runs. A particular homogeneous fluid coolant was used to fill the test apparatus and run freely without heat load first for cycle degas each time the coolant changed. After activating the circulating pump, the cooling fan on the air radiator side was turned on. The test specimen was checked to be aligned with the microchannel heat sink, and both were fixed together solidly with thermal paste. The electric heater was then adjusted using a voltage regulator to supply the required heat load to the specimen, as both simulate microprocessor loads. The flow velocity was tracked as measured by the flowmeter, and the flow velocity was adjusted using the control ball valve. The analog pressure sensors were used to record the pressure difference across microchannels, and the heat flux was adjusted incrementally to reach the desired value to be studied. The average temperature for the three measurements of each level of thermocouples in the test specimen was recorded as T_1 and T_2 for the upper and lower levels, respectively, as it was used to calculate the heat flux value through the specimen by Eq. (10). The heat flux supplied was calculated in each step using different methods: as electric energy from a voltage regulator reading supported on the specimen, then by Fourier's equation of heat conduction, where k_{sp} is the thermal conductivity of the test specimen material. The temperature gradient line is mathematically extrapolated to yield the specimen-coolant interface temperature T_s. The coolant mean temperature T_m is the average temperature of the inlet fluid and the outlet fluid, T_{in} and T_{out}. In addition, mean inlet flow velocity and mass flow rate were evaluated by flow rate measurements to assess and calculate the heat flux from the coolant side by Eq. (11). Moreover, by using the measured pressure difference, we could evaluate friction factor and pumping power using Eq. (12) and Eq. (13). As a result, (T_s-T_m) could be assessed for further calculations:

$$Q_S = \frac{k_{sp}A_{cr_{sp}}\Delta T}{x} \tag{10}$$

$$Q_c = \dot{m}_{nf}c_{p_{nf}}\left(T_{out} - T_{in}\right) \tag{11}$$

$$\Delta p = f\,\frac{v_m\rho_{nf}l}{2d_h} \tag{12}$$

$$\Omega = \dot{V}_{nf}\Delta p \tag{13}$$

where the subscriptions previously stated mean the following: *s* means surface, *c* means coolant, *m* means mean, *h* means hydraulic and *nf* means nanofluid.

The heat flux at the coolant side and the surface area of the microchannel heat sink were used to evaluate the heat transfer coefficient of the coolant utilized in the microchannel using Eq. (14). Furthermore, dimensionless parameters like Nusselt and Reynolds, could be easily evaluated and calculated using Eq. (15) and Eq. (16), respectively. They are vital for analyzing fluid behavior thermodynamically:

$$h = \frac{Q_c}{A_s(T_s - T_m)} \tag{14}$$

$$\mathrm{Nu} = \frac{hd_h}{k} \tag{15}$$

$$\mathrm{Re} = \frac{\rho v_m d_h}{\mu} \tag{16}$$

Finally, to evaluate the effect of using different types of nanofluids and hybrid nanofluids, the collective heat transfer coefficient ratio and Nusselt number ratio must be evaluated to assess the enhancement of the diminished value of employing different types of nanofluids and hybrid nanofluids using Eq. (17) and Eq. (18), respectively. Furthermore, for evaluating the overall performance of utilizing nanofluids hydrothermally, thermal performance evaluation criteria were used and calculated using Eq. (19) [9]:

$$h_r = \frac{h_{nf} - h_{bf}}{h_{bf}} \tag{17}$$

$$\mathrm{Nu}_r = \frac{\mathrm{Nu}_{nf} - \mathrm{Nu}_{bf}}{\mathrm{Nu}_{bf}} \tag{18}$$

$$\mathrm{PEC} = \frac{\mathrm{Nu}_{nf} / \mathrm{Nu}_{bf}}{f_{nf} / f_{bf}} \tag{19}$$

The next step after data reduction and calculation was uncertainty analysis and experimental validation, which analyzes derived quantities that depend on the uncertainties in experimentally measured quantities like pressure, temperature, microchannel dimensions, and flow rate using pressure transducers, *k*-type temperature sensors, micrometers, and electronic flow meters, respectively. Using the uncertainties of measured variables (W_1, W_2, ..., W_n), the uncertainties (W) of dependent variables (heat transfer coefficient, etc.) have been estimated by Kline and McClintock Eq. (20) [24] where R is a function of independent variables (X_1, X_2..., X_n). Followed by Table 5, showing the parameters and their uncertainty calculated values by comprehensive error analysis, so one has:

$$W = \pm\left[\left(\frac{\delta R}{\delta X_1}W_1\right)^2 + \left(\frac{\delta R}{\delta X_2}W_2\right)^2 + \ldots\ldots + \left(\frac{\delta R}{\delta X_n}W_n\right)^2\right]^{1/2} \tag{20}$$

By following the energy's path, it passed through a voltage regulator, an electric heater, a test specimen rod, then to microchannel heat and the coolant side, and then the heat was rejected to the surrounding area by an air heat exchanger. By comparing the calculated heat energy at each step, the test rig was validated as shown in Fig. 6, which represents the values of distilled water for the highest and lowest heat loads tested, and it showed that, for all heat flux ranges used in the experiments, the energy recorded from the voltage regulator was on average between 9.4% and 15.7% of the heat flux generated within the specimen and the heat transferred to the coolant fluid.

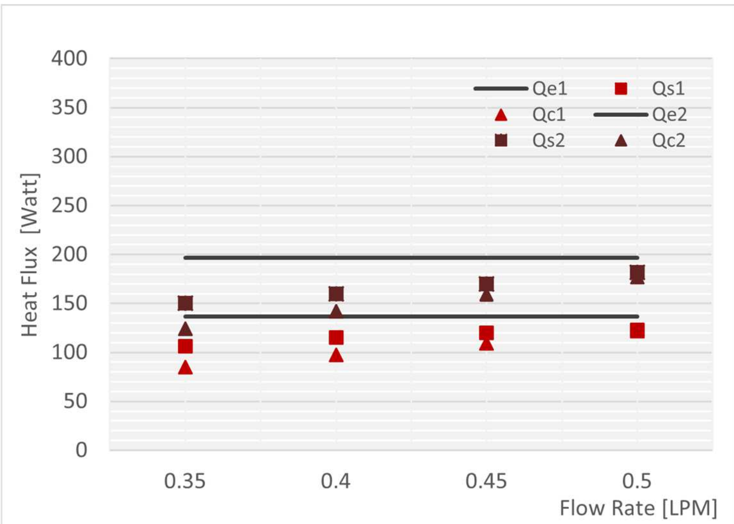

Fig. 6. Energy flow comparison for test rig experimental validation at Q = 196.4 W and Q = 136.4W.

Table 5. Experimental uncertainty values and error analysis for investigated parameters.

Parameters	$\lvert \delta X_1 \rvert \lvert X_1 \rvert$	$\lvert \delta X_2 \rvert \lvert X_2 \rvert$	$\lvert \delta T_1 \rvert \lvert T_1 \rvert$	$\lvert \delta T_2 \rvert \lvert T_2 \rvert$	$\lvert \delta T_s \rvert \lvert T_s \rvert$	$\lvert \delta T_m \rvert \lvert T_m \rvert$
% Uncertainty ±	0.2	0.4	0.167	0.154	0.525	0.716
Parameters	$\lvert \delta(T_s - T_m) \rvert \lvert (T_s - T_m) \rvert$	$\lvert \delta Q \rvert \lvert Q \rvert$	$\lvert \delta h \rvert \lvert h \rvert$	$\lvert \delta d_h \rvert \lvert d_h \rvert$	$\lvert \delta \dot{V} \rvert \lvert \dot{V} \rvert$	$\lvert \delta Nu \rvert \lvert Nu \rvert$
% Uncertainty ±	0.89	14.203	15.02	8.27	13.69	17.148

Table 6. The parameters studied through the experiment and their specific values.

Parameters	Value	Unit
Heat flux	136.4, 158.2, 180, 196.4	Watt
Flow rate	0.35, 0.4, 0.45, 0.5	LPM
Nanoparticle types/ base fluid	Al_2O_3, ZnO, CuO, and Ag/ distilled water	-
Mixture ratio	50%, 33.3%, and 25% for di, tri, and tetra, respectively.	Per volume
Concentration in the base fluid	0.025% ,0.05%	Per volume
Width of channel	117	µm
Geometric parameters	- Rectangular cross-sectional - Multiple channels - Straight configuration - Linear array	-

Besides, the repeatability of readings taken by the device was examined by distilling water for a particular condition, and readings were taken every 15 minutes to determine the time needed to reach a steady state. It typically takes one hour, and the longest time ever recorded was 1.25 hours. To ensure reaching a steady state, all recorded values were taken 1.5 hours later. In contrast, the same parameters for distilled water were recorded and tested four times in a row. Nusselt number is an important parameter, which shows the heat transfer performance in non–dimensional form. The percentage of standard error was calculated and found to be less than 4.7% as shown in Fig. 7, which was an accepted margin [8]. Nusselt results showed good agreement with data reported by Kandlikar for pure water [13, 46, 47].

3. Results and Discussion

In this study, we investigate the intricate interplay between various parameters affecting heat transfer through microchannel heat sink. Specifically, we delve into the effects of manipulating heat load, flow velocity, micro-concentration of nanoparticles, and fluid flow friction factor to comprehensively assess the hydrothermal performance of nanofluids and hybrid nanofluids under diverse conditions. By systematically varying these parameters, we aim to elucidate their individual and collective impacts on heat transfer coefficient and Nusselt number. Subsequently, we evaluate the performance of the tested nanofluids and hybrid nanofluids using established performance evaluation criteria. This approach allows for an understanding of the hydrothermal behavior and performance characteristics of the investigated fluids. Finally, as the parameters tested in the current study are many, they must be illustrated and represented together before representing the results and findings or conducting any further analysis, as shown in Table 6. The parameters tested through the study were highlighted and represented together.

There is no doubt that the heat loads and fluid flow rates have an impact on the Nusselt number and heat transfer coefficient of the working coolant in microcooling systems. For example, by employing tetra-hybrid nanofluid, as shown in Fig. 8(a), changing heat loads at different flow velocities showed an increasing trend on Nusselt number and heat transfer coefficient; however, the change percentage is different based on the coolant type used. Moreover, as shown in Fig. 8(b), manipulating flow velocity in terms of Reynolds number showed an increasing trend in Nusselt number and heat transfer coefficient. However, each fluid showed a different enhancement percentage with the manipulated heat loads and flow rates. Likewise, all other coolant types showed the same trend; however, each type has a unique magnitude of enhancement.

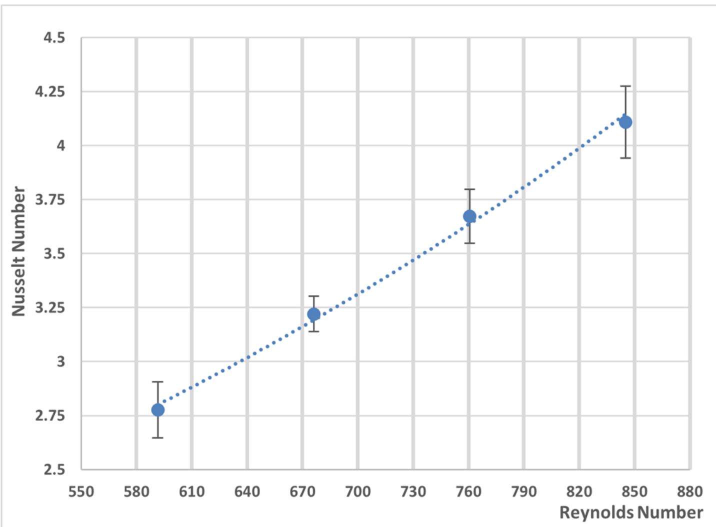

Fig. 7. Percentage of standard error around the mean value based on standard deviation of a sample of four measurements of distillated water at Q = 136.4 Watt and flow rate range from 0.35 to 0.5 LPM.

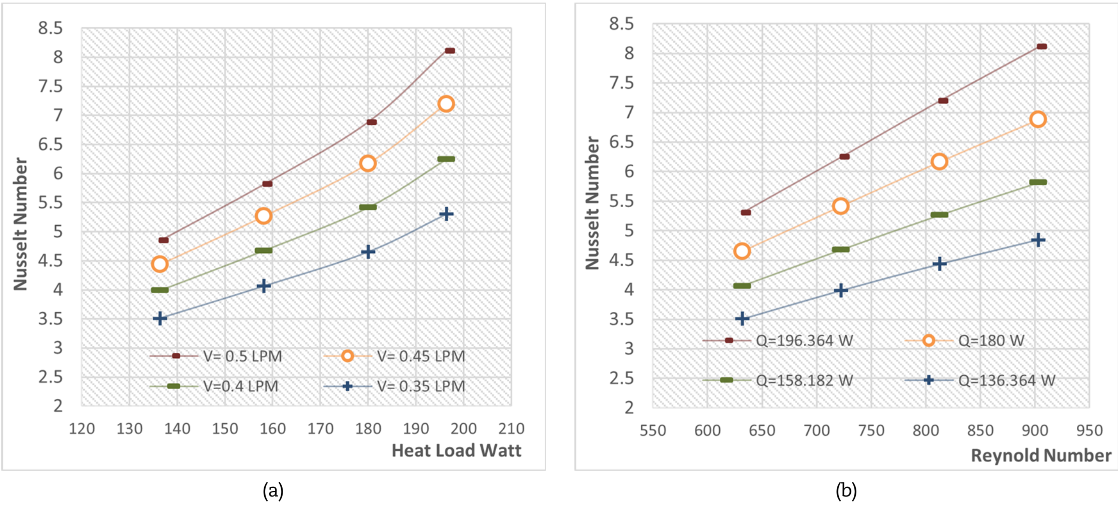

Fig. 8. Nusselt number variation utilizing tetra-hybrid nanofluid at φ = 0.025% per volume, (a) Nu versus heat load, (b) Nu versus Re.

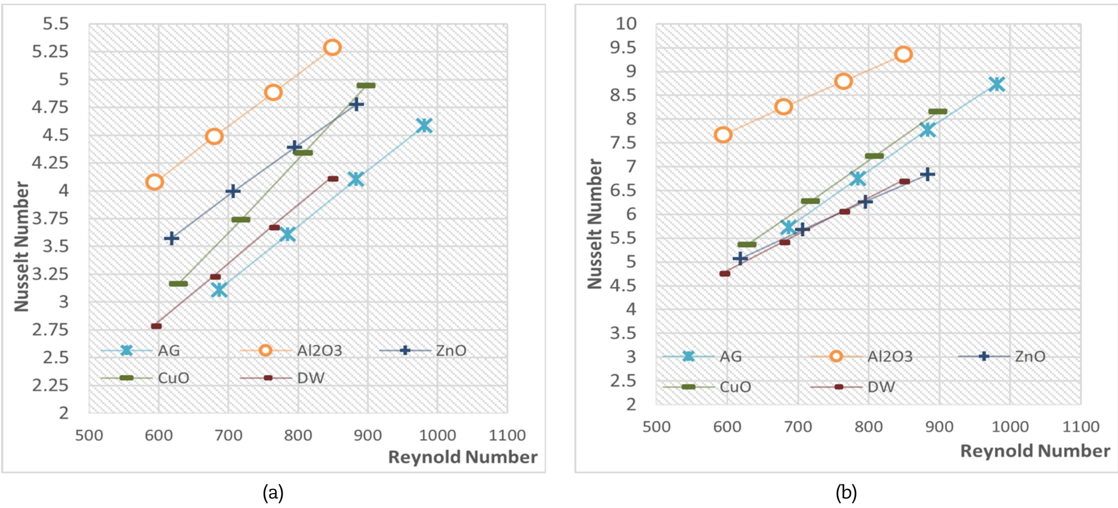

Fig. 9. Nusselt number versus Reynold number for mono nanofluids at heat loads, (a) 136.4 W, (b) 194.4 W, and concentration of φ = 0.025% per volume.

3.1. Effect of nanofluids and hybrid nanofluids up to tetra-level on heat transfer coefficient

In the subsequent segment, the Nusselt number is graphed against the Reynolds number for every kind of nanofluid and its hybridizations at the particular micro-concentration examined (φ= 0.025% per volume) to examine their impact on thermal performance and heat transfer properties while simultaneously adjusting operating conditions. As illustrated in Figs. 9, 10, and 11, three figures describe each stage of hybridization, from mono- to tetra-nanofluids, detailing how each performs in terms of the Nusselt number with the variation of the Reynolds number. Additionally, each figure has two sections that illustrate the performance of nanofluids at various heat loads, 136.4 and 194.4 watts. Al_2O_3 mono-nanofluid had the highest Nusselt number and the best heat transfer coefficient enhancement among all tested mono-nanofluids at all tested heat loads, as illustrated in Fig. 9. The worst coolant, however, is still up for debate because it varies depending on the applied load. ZnO nanofluid fared reasonably well at the lowest heat load because its values trail Al_2O_3 nanofluid in terms of enhancement levels, but it recorded the lowest overall value at the highest heat load because its values were as close to pure water values. Conversely, Ag nanofluid demonstrated lower Nusselt number values at lower heat loads when compared to pure water; nevertheless, as the heat load is increased, its performance improves noticeably, particularly at higher Reynolds number ranges, as they approach Al_2O_3 nanofluid values. Additionally, CuO nanofluids demonstrated consistent performance under varying heat loads, demonstrating a good enhancement range over pure water, and this performance improved with increasing Reynolds number. Except for Ag nanofluid at low heat load ranges, all mono-nanofluids generally outperformed pure water.

On the other hand, as the heat load increased, all di-hybrid nanofluids generally displayed an increase in Nusselt values relative to pure water, as illustrated in Fig. 10. But it's important to note that, at a low heat load of 136.4 watts, ZnO-Ag and CuO-Ag demonstrated the lowest enhancement level of all the tested di-nanofluids. However, both enhancement values significantly increased along with an increase in Reynolds number as the heat load increased. Conversely, at low heat loads, Al_2O_3-Ag demonstrated and recorded a higher enhancement level, and at higher heat loads, its heat performance deteriorates. The Nusselt number of all tested di nanofluids at φ = 0.025% per volume micro-concentration showed higher values when heat load was increased compared to pure water; their levels of enhancement are comparatively close to one another. Furthermore, the di-hybrid nanofluids' Nusselt number values exceeded those of the mono-nanofluids, except for Al_2O_3. This indicates that hybridizing other particles with Al_2O_3 resulted in a notable improvement in their Nusselt number values. Consequently, at the di-hybrid level, the new blind benefits from both entities within; however, it is unclear which benefit will predominate more as it may also depend on the hybridization ratio and operating conditions.

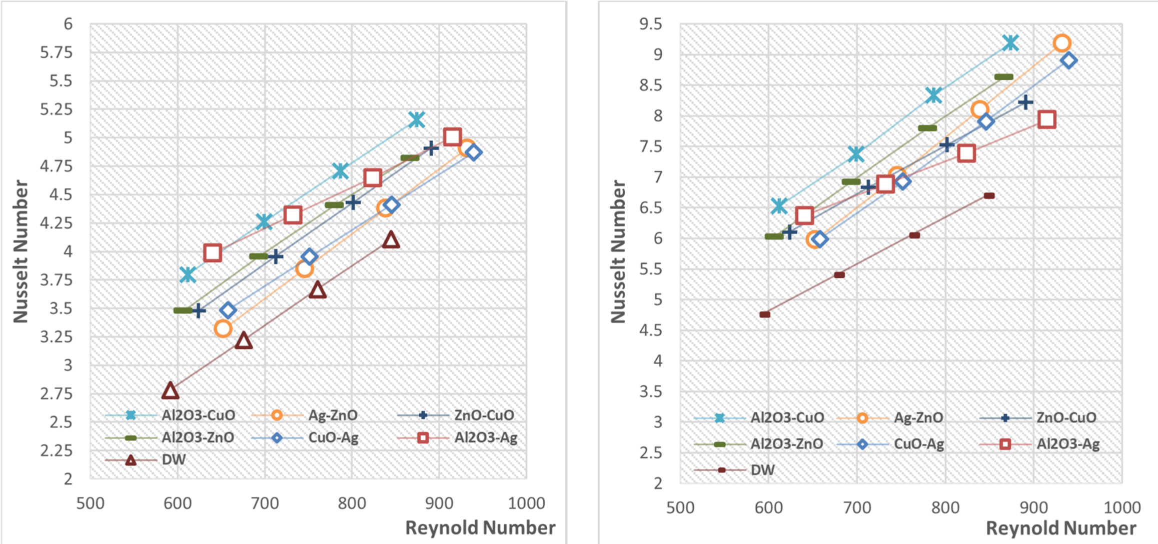

(a) (b)

Fig. 10. Nusselt number versus Reynold number for di hybrid nanofluids at heat loads, (a) 136.4 W, (b) 194.4 W, and concentration of φ = 0.025% per volume.

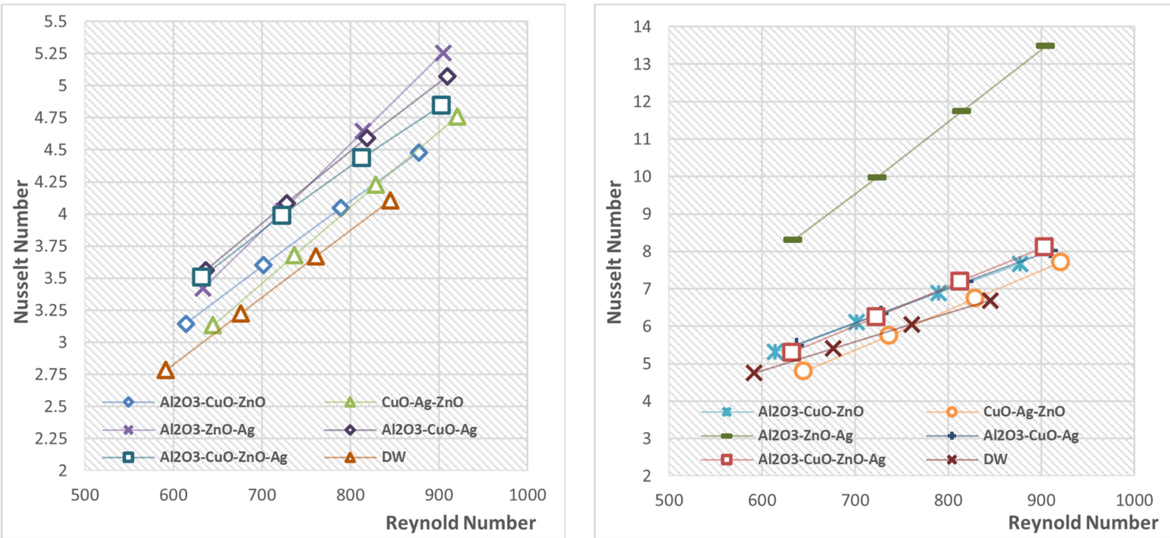

(a) (b)

Fig. 11. Nusselt number versus Reynold number for tri and tetra hybrid nanofluids at heat loads, (a) 136.4 W, (b) 194.4 W, and concentration of φ = 0.025% per volume.

Additionally, at 136.4-watt heat load, as illustrated in Fig. 11(a), Al_2O_3-ZnO-Ag and Al_2O_3-CuO-Ag tri-nanofluids exhibited the best performance among tri and tetra nanofluids; nonetheless, as heat flux escalated, Al_2O_3-ZnO-Ag Nusselt number demonstrated a remarkable enhancement and recorded the highest enhancement value overall test nanofluids. On the other hand, CuO-ZnO-Ag recorded the lowest enhancements at lower heat loads, but it performed better than pure water in terms of Nusselt value; nevertheless, as Fig. 11(b) shows, at higher heat loads, its thermal performance deteriorates, and it shows lower values of Nusselt numbers than pure water, particularly at lower Reynolds numbers. The difference in structure, particle size, thermal conductivity, and overall density of the Al_2O_3-ZnO-Ag combination may be the cause of this enhancement, as the Soret and Dufur effects are maximum in this combination. Soret phenomena mean different components of a multicomponent system move at a different rate in response to temperature gradients, creating a concentration gradient followed by the Dufour effect, which means that the concentration gradient leads to better energy transfer associated with such systems. Furthermore, the Al_2O_3-ZnO-Ag combination demonstrated the capacity to overcome the disadvantages of each type within its blend and performed better than other combinations thermally. The performance of other hybrid nanofluids, such as Ag-CuO, CuO-ZnO, and ZnO-Ag, was consistently poor because of the negative effects of their hybridization compared to their mono-nanofluid enhancement values.

3.2. Effect of heat flux utilizing nanofluids on heat transfer coefficient and Nusselt number

Generally, at φ = 0.025% volume, all tested nanofluids showed higher values of heat transfer coefficient and Nussult number over pure base fluid at all of the operating conditions tested in the experiment. Furthermore, as shown in Figs. 12 and 13, Nusselt numbers versus heat loads were plotted at φ = 0.025% per volume for the highest flow rate of 0.5 LPM and the lowest flow rate of 0.35 LPM, respectively. Each figure contains three parts presenting a level of hybridization: (a) for mono-nanofluids, (b) for di-hybrid nanofluids, and (c) for tri- and tetra-hybrid nanofluids. At 0.5 LPM, as shown in Fig. 12(a), the findings were as follows: Al_2O_3 nanofluid showed the highest value of Nusselt number with increasing heat flux, while ZnO showed the lowest among mono nanofluids. Besides, Ag nanofluid showed the highest exponential increase in the percentage of Nusselt number among them all. It is noticeable that metal-based nanofluids showed thermally better enhancement jumps with increasing heat load than metal oxide-based nanofluids. The variation in enhancement values of each type of nanofluid might be for a different reason, as particle nature affects its reaction to manipulating the heat load. Al_2O_3 nanoparticles with a lower density and a more consistent crystalline structure fill the gaps in the water's tetrahedral structure better, which increases micro-convectional heat diffusion. Ag nanoparticles, on the other hand, have a higher density and thermal conductivity, which enhances particulate momentum and collisions, resulting in higher heat diffusion. Moreover, as shown in Fig. 12(b), for di hybrid nanofluids, ZnO-Ag recorded the highest increase in enhancement percentage with increasing heat load, while Al_2O_3-CuO nanofluid showed the highest value of Nusselt number among di nanofluids tested. On the other hand, the combinations of Al_2O_3-Ag and CuO-ZnO hybrid nanofluids showed the lowest Nusselt values and heat transfer coefficients among di nanofluids. Moreover, as shown in Fig. 12(c), the heat transfer performance of tri- and tetra-hybrid nanofluids with changing heat loads was as follows: For all tested combinations of nanoparticles used, the Al_2O_3-ZnO-Ag hybrid nanofluid showed the highest value and the highest increase in the percentage of Nusselt number. Conversely, CuO-ZnO-Ag displayed the lowest Nusselt number. Each component within hybrid blends appears to be beneficial, but it's unclear which benefit will predominate more.

As illustrated in Fig. 13, all tested coolants exhibit distinct behaviors at 0.35 LPM for variations in the subjected heat load, in contrast to high flow rates. However, as shown in Fig. 13(a) and (c), the exceptions are the Al_2O_3 mono nanofluid and the Al_2O_3-ZnO-Ag-tri hybrid nanofluid, which also exhibited similar thermal performance. On the other hand, ZnO nanofluid demonstrated its best thermal performance at lower heat loads and flow rates, despite showing the least increase in Nusselt percentage among mono-nanofluids as the heat flux increased. So, the thermal conductivity of nanoparticles had a clear effect, especially at higher heat load values. Conversely, Al_2O_3-Ag, followed by Al_2O_3-CuO di-nanofluids, recorded the highest values of Nusselt number among the tested di-nanofluids; however, it is noticed that at a higher flow velocity, Al_2O_3-CuO showed a slightly higher Nusselt number. On the contrary, ZnO-Ag at low flow velocity showed the lowest value of Nusselt enhancement among di-nanofluids. The findings of di-hybrid nanofluids promote the reason stated earlier, as ZnO-Ag and Al_2O_3-Ag switched their behavior at low flow rates. Furthermore, tri and tetra hybrid nanofluids reported the same thermal performance despite the flow rate value, as Al_2O_3-ZnO-Ag showed the best Nusselt enhancement and CuO-ZnO-Ag showed the worst enhancement values among tested tri and tetra hybrid nanofluids; however, their magnitude of enhancement compared to pure base fluid was different.

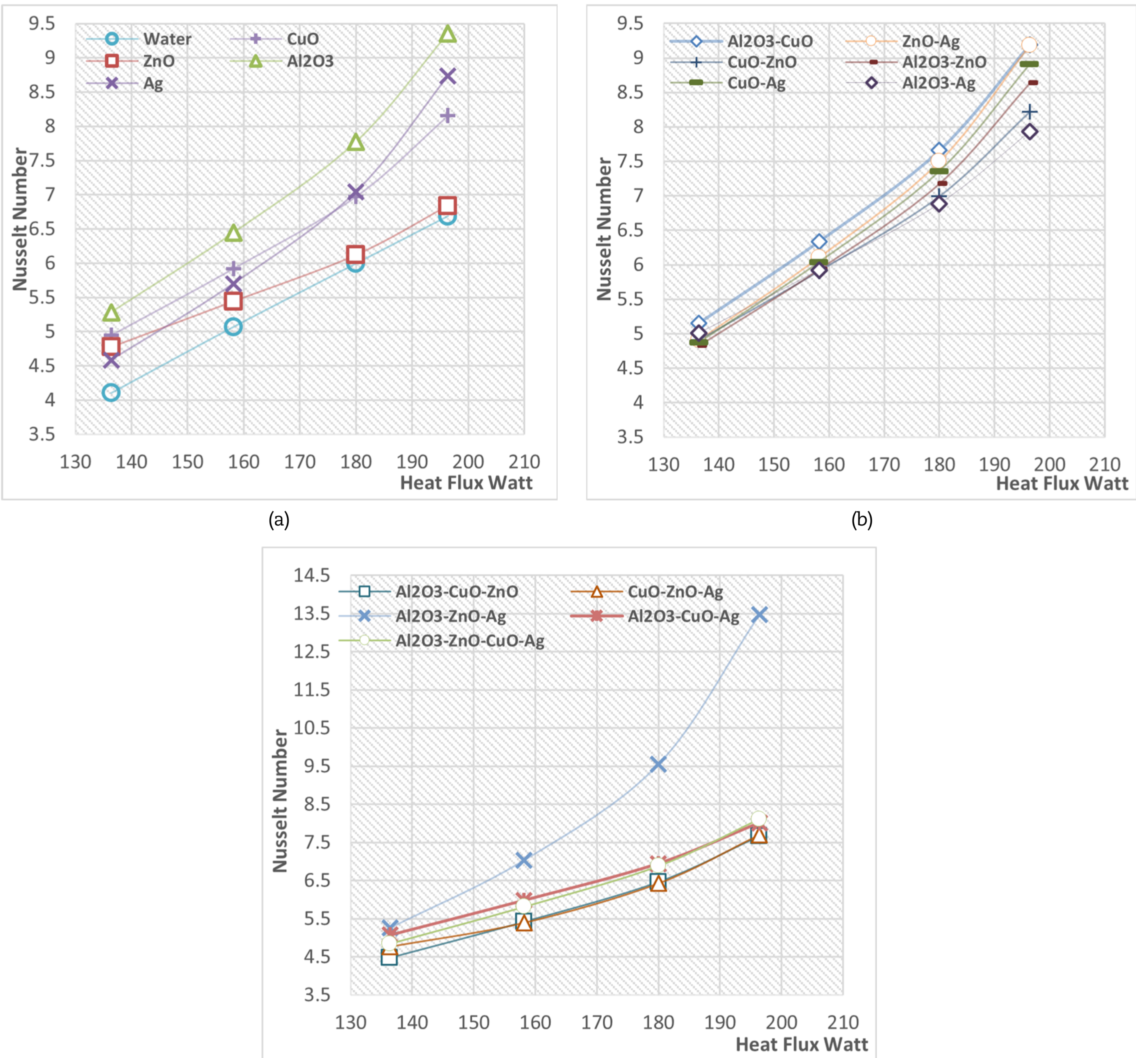

(c)

Fig. 12. Nusselt number versus heat loads at the highest flow rate of 0.5 LPM and φ = 0.025% per volume, (a) mono-nanofluids, (b) di-nanofluids, (c) tri and tetra-nanofluids.

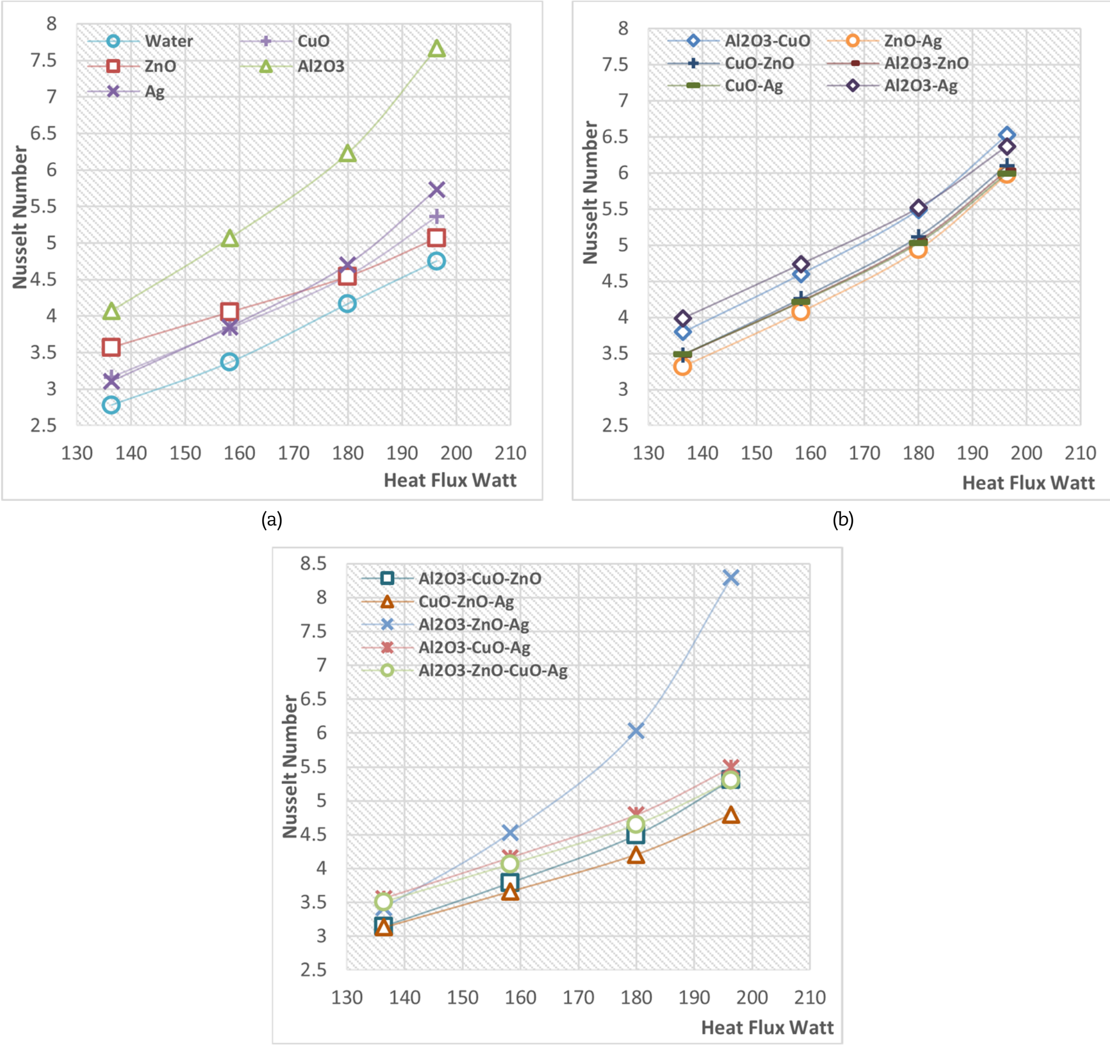

Fig. 13. Nusselt number versus heat loads at the highest flow rate of 0.35 LPM and φ = 0.025% per volume, (a) mono-nanofluids, (b) di-nanofluids, (c) tri and tetra-nanofluids.

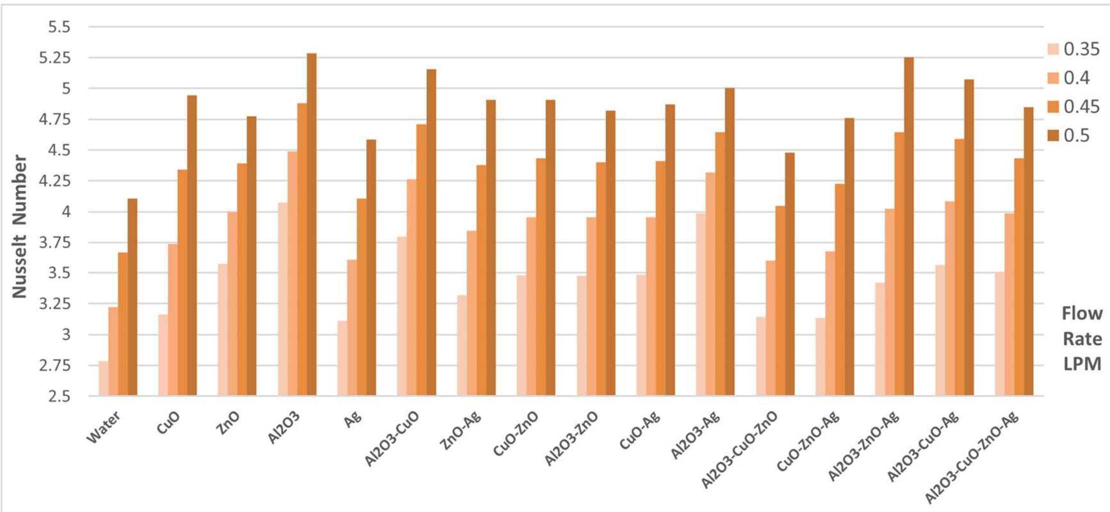

Fig. 14. Nusselt number versus nanofluid type at different flow rates at a low heat load of 136.4-Watt and concentration of 0.025% per volume.

Heat transfer by micro-convection could be promoted with a more consistent nanoparticle molecular crystal structure compared to the base fluid; thus, the corundum structure and triagonal shape of the Al_2O_3 molecular bonding, which are more cohesive with the tetrahedral geometry of water molecular bonding, promoted micro-convection within the fluid flow. However, its lower increment in enhancement percentage when increasing coolant flow velocity compared to other nanoparticles might be due to the relatively lower density and particle size, which decrease particle momentum and its ability to cause higher particle collisions.

3.3. Effect of flow velocity utilizing nanofluids on heat transfer coefficient and Nusselt number

The differences between Nussult number values while increasing the flow rate must be illustrated to evaluate how manipulating flow rates affects its enhancement. As shown in Figs. 14 and 15, at φ = 0.025% per volume, the Nusselt number is plotted for all types of coolants, illustrating its variation with coolant flow velocity from 0.35 to 0.5 LPM at the lowest and highest heat loads, respectively. Furthermore, at the lowest heat load of 136.4 watts, as shown in Fig. 14, CuO followed by Ag mono-nanofluids showed the highest difference in Nusselt values by increasing the coolant flow rate, while ZnO and Al_2O_3 showed the lowest difference in Nusselt values, even lower than the values of the base fluid. Moreover, for di nanofluids, ZnO-Ag followed by CuO-ZnO showed the highest difference in Nusselt values by increasing the coolant flow rate, while Al_2O_3-Ag showed the lowest difference in Nusselt values, even lower than the values of the base fluid. Additionally, for tri- and tetra-nanofluids, the Al_2O_3-ZnO-Ag tri-hybrid showed the highest difference in Nussult values, not only over tri-nanofluids but also among all tested combinations. Al_2O_3-CuO-ZnO and tetra nanofluid showed the lowest difference in Nusselt values among tri and tetra nanofluids, almost the same as the values of the base fluid. Generally, tri nanofluids showed a higher difference in Nusselt values than di nanofluids; besides, di nanofluids were higher than mono nanofluids except for CuO mono-nanofluid, which comes after Al_2O_3-ZnO-Ag tri hybrid nanofluid values.

Conversely, at the highest tested heat load of 196.4 watts, as shown in Fig. 15, Ag followed by CuO showed the highest difference in Nusselt values by increasing the coolant flow rate, while Al_2O_3 showed the lowest difference in Nusselt values; however, all were higher than the values of the base fluid. Moreover, for di-nanofluids, ZnO-Ag, followed by CuO-Ag, showed the highest difference in Nusselt values by increasing the coolant flow rate, while Al_2O_3-Ag showed the lowest difference in Nusselt values; however, all were higher than the values of the base fluid as well. Additionally, for tri- and tetra-nanofluids, Al_2O_3-ZnO-Ag showed the highest difference in Nusselt values over all tested combinations at all operating conditions. Al_2O_3-CuO-ZnO showed the lowest difference in Nusselt values, and all were higher than the values of the base fluid. Generally, all nanofluids showed a higher difference in Nusselt values than base fluid values. In contrast to pure water, which recorded a lower difference, all nanofluids improved the difference in Nusselt values at the highest tested heat load by increasing the flow rate, pointing out that neither the Reynolds number nor the friction factor have been covered yet, as doing so will provide a complete perspective of how each nanofluid acts hydrothermally overall.

Generally, increasing heat load magnifies the enhancement ability of nanofluids by increasing their flow rate. Moreover, nanoparticles with a relatively higher density and larger particle size provide a higher collision possibility, which leads to a higher magnitude of particle momentum. Thus, Ag and CuO mono-nanofluids showed a higher Nusselt difference with increasing flow rate at higher levels of heat loading. When heat load increases at higher flow rates, it stretches molecular gaps, increasing the probability of particle-to-particle collisions and, ultimately, particle momentum, which in turn increases the thermal conductivity effect of nanoparticles. This is the Nusselt enhancement mechanism of nanofluids. Besides, having a more dissimilar crystal structure than the base fluid results in a reduction in the heat transfer potential through microconvention. This may also account for the consistently higher values of enhancements observed in the behavior of Al_2O_3-CuO and Al_2O_3-Ag di-hybrid nanofluids, as they gain from the advantages of each particle's higher micro-convention and particle-to-particle momentum.

3.4. Effect hybridizations of mono nanofluids on their thermal Performance

The subsequent section will address the hybridization of each mono-nanofluid with the others and how this influences the values of Nusselt numbers. The Nusselt number is plotted against each mono-nanofluid and its different hybridizations in Figs. 16, 17, 18, and 19 at a maximum flow rate of 0.5 LPM. Each figure is divided into two sections, (a) and (b), which show the highest and lowest heat loads, respectively. As can be seen in Fig. 16, when utilizing Al_2O_3 mono nanofluid as the base nanofluid, hybridizing it with any other kind of particle had an adverse effect on its Nusselt number values at the di, tri, or even tetra level of hybridization, particularly when the heat load was low. However, combining ZnO and Ag particles to create a tri-hybrid nanofluid showed a discernible benefit at higher heat flux levels. On the other hand, for all heat loads, the CuO and ZnO mixture had the largest negative impact on its Nusselt number values and heat transfer coefficient.

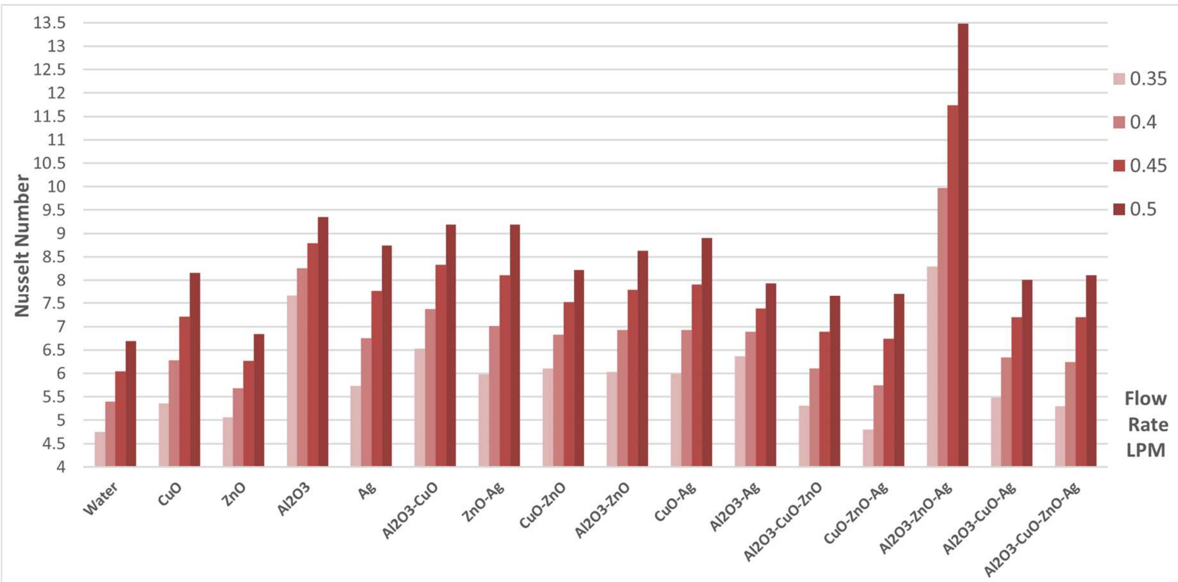

Fig. 15. Nusselt number versus nanofluid type at different flow rates at the highest heat load of 196.4 watts and concentration of 0.025% per volume.

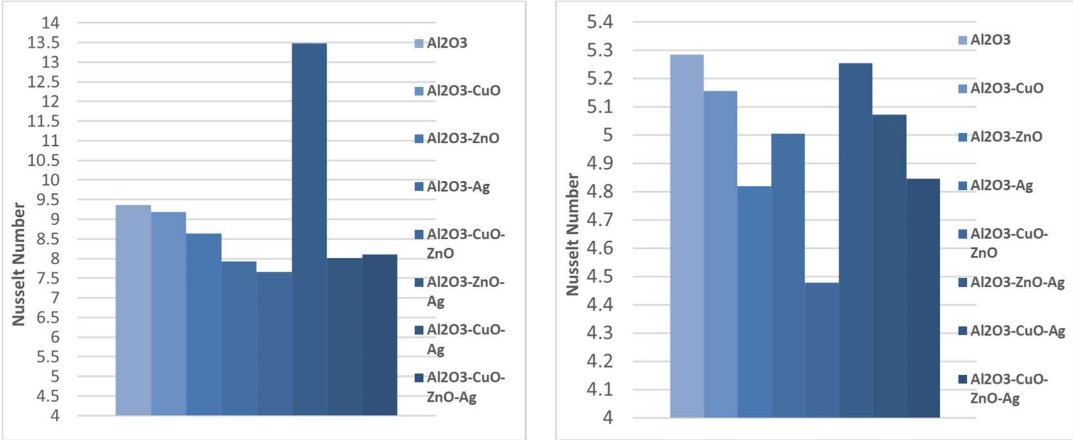

(a) (b)

Fig. 16. Nusselt number versus Al_2O_3 nanofluid and its hybridization at 0.5 LPM flow velocity and heat load, (a) 194.4 W, (b) 136.4 W, and concentration of φ = 0.025% per volume.

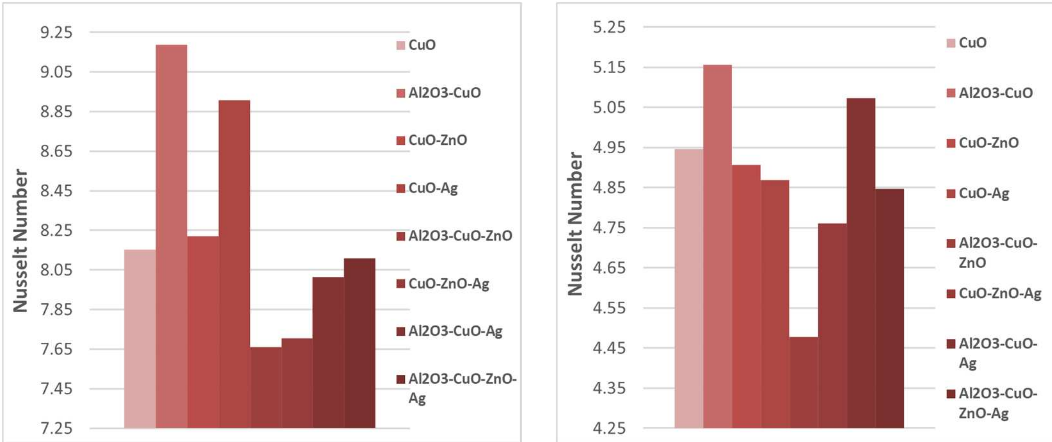

(a) (b)

Fig. 17. Nusselt number versus CuO nanofluid and its hybridization at 0.5 LPM flow velocity and heat load, (a) 194.4 W, (b) 136.4 W, and concentration of φ = 0.025% per volume.

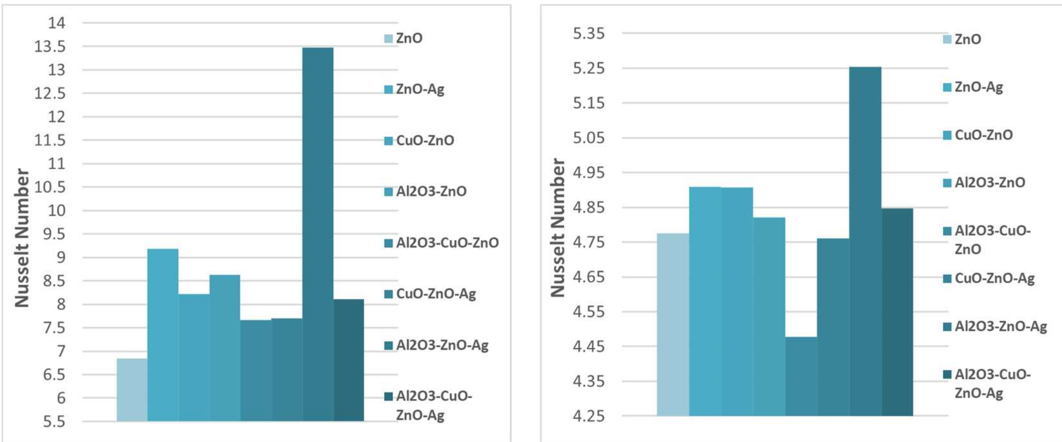

(a) (b)

Fig. 18. Nusselt number versus ZnO nanofluid and its hybridization at 0.5 LPM flow velocity and heat load, (a) 194.4 W, (b) 136.4 W, and concentration of φ = 0.025% per volume.

Figure 17 illustrates the hybridization effect of CuO mono nanofluid at both the highest and lowest heat loads through the addition of other particles. The addition of Al_2O_3 or Ag nanoparticles to the CuO hybridization process at the di-hybrid level produced the greatest enhancement in Nusselt values at the highest heat load, as illustrated in Fig. 17(a). The values obtained from the other combinations were lower than those obtained from the CuO mono nanofluid. Tri-hybridizing with Ag and Al_2O_3 nanoparticles, followed by di-hybridizing with Al_2O_3 nanoparticles, demonstrated the greatest enhancement at the lowest heat load, while the other combinations displayed Nusselt values lower than CuO mono nanofluid values. Furthermore, of all the tested heat loads, tri-hybridization with the addition of ZnO and Al_2O_3 had the highest negative impact on the Nusselt number.

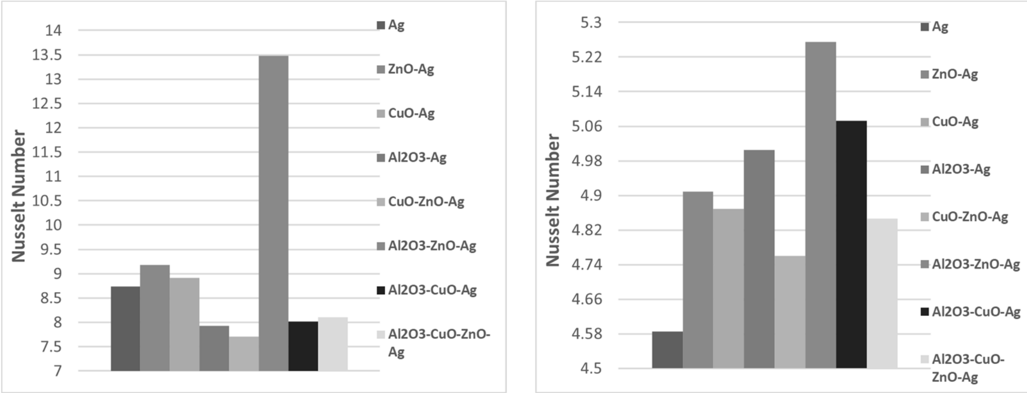

(a) (b)

Fig. 19. Nusselt number versus Ag nanofluid and its hybridization at 0.5 LPM flow velocity and heat load, (a) 194.4 W, (b) 136.4 W, and concentration of φ = 0.025% per volume.

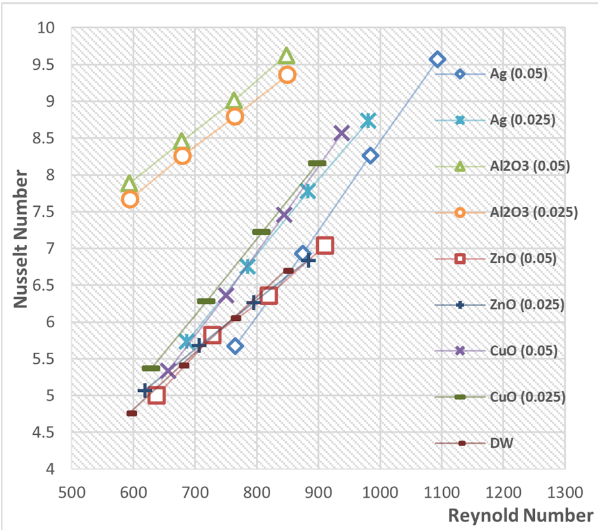

Fig. 20. Nusselt number vs. Reynold number for mono nanofluids at heat load of 194.4 W and concentration of φ = 0.025% and φ = 0.05% per volume.

Moreover, ZnO mono-nanofluid hybridization at varying heat loads, as illustrated in Fig. 18, revealed that, at low heat loads, all combinations—aside from ZnO-Al_2O_3-CuO and ZnO-Ag-CuO tri hybrid nanofluids—recorded higher Nusselt values; at higher heat loads, however, all combinations showed higher Nusselt number values over pure ZnO mono nanofluid. Furthermore, tri-hybridizing ZnO with Al_2O_3 and Ag nanoparticles showed the greatest increase in Nusselt number and was the most beneficial approach, especially when high heat loads were involved, besides, di-hybridizing ZnO with Ag nanoparticles came in second.

As illustrated in Fig. 19(b), hybridizing Ag mono-nanofluid with any other particle at the lowest heat load resulted in a noteworthy enhancement of Nusselt values. At maximum heat load, as illustrated in Fig. 19(a), only a few combinations (e.g., ZnO-Ag and CuO-Ag di-nanofluids) showed slightly higher Nusselt values over Ag mono-nanofluid; all other hybrid types showed lower Nusselt values than Ag mono-nanofluid Nusselt values, except Al_2O_3-ZnO-Ag, which also recorded the highest Nusselt values among all hybridized coolant fluids.

3.5. Effect of micro concentrations of mono and hybrid nanofluid on heat transfer coefficient

The effect of increasing nanofluid micro-concentration from φ = 0.025% to φ = 0.05% per volume will be covered in the following section, along with potential implications for heat transfer capabilities and the Nusselt number for coolant passing through a microchannel heat sink with a 117-micrometer channel size. Taking into consideration splitting the results for mono, di, tri, and tetra nanofluids to have a clear overview of how hybridization effects behave at different micro-concentration levels. As shown in Fig. 20, the Nusselt number versus the Reynolds number is plotted for all mono-nanofluids at both concentrations, focusing on the highest heat load tested. The heat transfer coefficient and Nusselt number of mono-nanofluids based on metal oxides increase with increasing nanoparticle concentration, and the degree of enhancement rises with an increase in Reynolds number. In contrast, metal-based nanofluids react oppositely, with Ag mono-nanofluid exhibiting a higher Nusselt number value at lower concentrations. Generally, all mono-nanofluids at the highest heat load tested showed enhancement values over pure base fluid; however, Ag mono-nanofluid was the exception only at a lower Reynolds number range.

Furthermore, all combinations of di hybrid nanofluids, as shown in Fig. 21, illustrated the Nusselt number versus Reynolds number for all di nanofluids at both micro-concentrations. In contrast, manipulating micro-concentration for di-hybrid nanofluids showed the opposite behavior to mono-nanofluids. As the micro-concentration level increased from φ = 0.025% to φ = 0.05%, the heat transfer coefficient and Nusselt number showed significantly diminished values, not only compared to the values at the lower concentration but also lower than pure water heat transfer coefficient and Nusselt number values. The retarding values of the Nusselt number and heat transfer performance due to increasing concentration were very noticeable. For di-hybrid nanofluids at the lower micro-concentration values, they recorded significant enhancement values over pure base fluid and mono nanofluids as well, except for Al_2O_3 mono-nanofluid, which showed a higher enhancement value over all tested di-hybrid nanofluids.

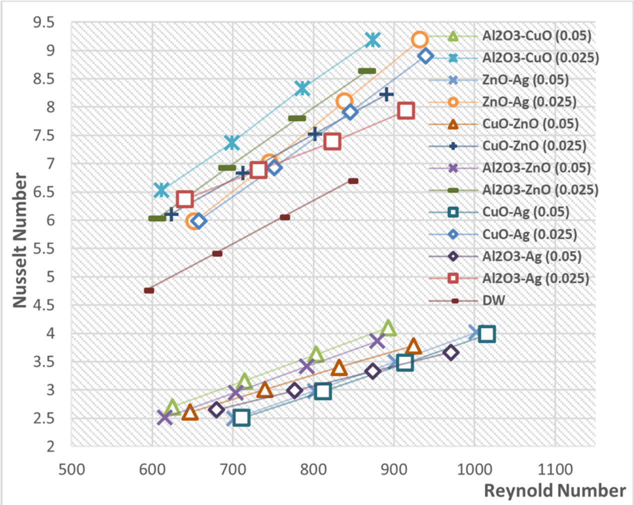

Fig. 21. Nusselt number versus Reynolds number for di nanofluids at a heat load of 194.4 W and concentration of φ = 0.025% and φ = 0.05% per volume.

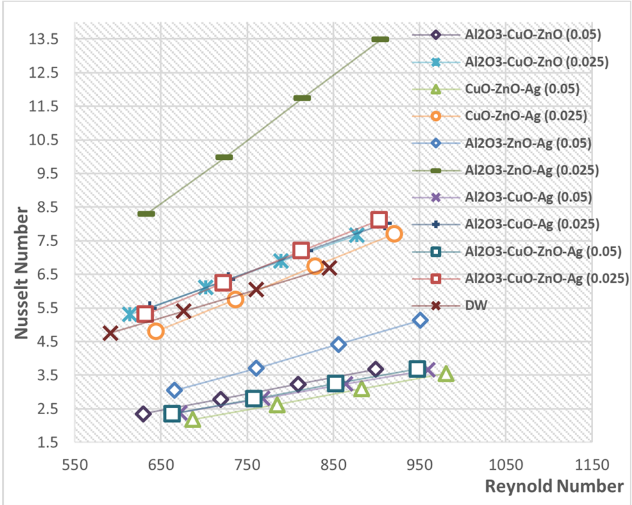

Fig. 22. Nusselt number versus Reynold number for tri and tetra nanofluids at a heat load of 194.4 W and concentration of φ = 0.025% and φ = 0.05% per volume.

Moreover, hybrid nanofluids at the tri and tetra levels of hybridization performed similarly to di hybrid nanofluids, as shown in Fig. 22. All types of tri and tetra hybrid nanofluids at lower concentrations showed enhanced values of Nusselt number and heat transfer coefficient over pure water, except CuO-ZnO-Ag tri nanofluid, especially at lower Reynolds number values; however, the magnitude of enhancement differs substantially. As the micro-concentration level increased from φ = 0.025% to φ = 0.05%, the heat transfer coefficient and Nusselt number showed significantly diminished values, not only compared to the values at the lower concentration but also lower than pure water values. For tri and tetra nanofluids at the lower micro-concentration level, despite recording enhancement values over pure base fluid, the enhancement values were insignificant compared to mono nanofluids and di-hybrid nanofluids as well, except Al_2O_3-ZnO-Ag tri hybrid nanofluid, which surprisingly recorded the highest values of Nusselt number and heat transfer coefficient among all nanofluids and hybrid nanofluids at a constant hybridization ratio. Additionally, the increment in enhancement percentage of di nanofluids was higher than most of the tri and tetra nanofluids, with a decreasing particle micro-concentration from φ = 0.05% to φ = 0.025% per volume.

The results using hybrid nanofluids with micro-concentration manipulation and nanofluids may be explained by the tendency of nanoparticles to form clusters when suspended in a liquid, a phenomenon known as particle clustering and agglomeration effects. This results in a pathway with reduced thermal resistance. It hasn't, as far as we know, been suggested for hybrid nanofluids, though. Furthermore, using hybrid nanoparticles might create hybrid clusters, whose size is a factor in the particle nature of hybridization. The relatively larger cluster size at higher concentrations creates a larger network of clusters, preventing each other from passing through the microchannel gaps of 117 micrometers. This causes an increase in thermal resistance between the heat sink and fluid flow. In contrast, using a lower micro-concentration level results in a lower cluster rate, which allows hybrid nanoparticles to permeate through microchannels, reducing the thermal resistance and improving the overall heat transfer capabilities. From the perspective of the nanofluid, on the other hand, increasing concentration with comparatively smaller cluster sizes increases its rate within microchannels; consequently, it offers a higher heat transfer capability in addition to decreasing the free gaps within the base fluid, which also facilitates heat transfer.

3.6. Performance evaluation criteria and effect of friction factor for MCHS using nanofluids

In addition to examining the coolant's heat transfer capabilities, it is imperative to analyze and discuss pressure drop, fluid friction factor, and pumping power across a heat sink when assessing the coolant's overall performance. As shown in Fig. 23, pressure drop across microchannels using different types of coolants, starting with pure water up to tetra hybrid nanofluid, is illustrated at different flow rates conducted in the experiment. The figure showed that as the flow rate increased, the pressure drop increased; however, the increment range increased noticeably as the flow rate increased more than 0.4 LPM for all types of coolants. In addition, nanofluids showed a higher percentage increase in pressure drop as the flow rate increased over pure base fluid. Additionally, it was noticed that di-hybrid nanofluids showed a pressure difference range relatively lower than mono, tri, and tetra nanofluids, except for Al_2O_3 mono nanofluid, which showed the lowest pressure difference among all nanofluid combinations. Moreover, there is no recorded change in pressure drop with changing heat flux across the tested parameters of the experiment.

For further analysis, as shown in Fig. 24, the friction factor is plotted against the Reynolds number, showing how fluid flow behaves when different types of coolant are used. As illustrated in Fig. 24, it showed the variation of friction factor against Reynolds number at φ = 0.025% per volume for mono-nanofluids in Fig. 24(a), di-nanofluids in Fig. 24(b), and tri- and tetra-nanofluids in Fig. 24(c); Al_2O_3 nanofluid showed the lowest friction factor, and Al_2O_3-CuO-ZnO showed the highest friction factor among them all. Additionally, all tri and tetra nanofluids showed a higher friction factor than mono and di nanofluids; Al_2O_3-ZnO-Ag tri-nanofluid behaved differently and showed relatively lower friction factor values. It is noticed that Ag mono nanofluid has the highest friction factor among all mono nanofluids; however, its hybridizations decrease its friction factor values. Moreover, as concentration increased, the friction factor increased for all types of nanofluids and hybrid nanofluids at any level of hybridization.

Equation (26) shows the ratios between the fluid friction factor across microchannels and the Nusselt number ratio when employing nanofluids in terms of hydrothermal performance. Performance evaluation criteria were plotted against Reynolds numbers, as shown in Figs. 25, 26, and 27. Each figure had two parts, (a) and (b), to illustrate the performance of mono-, di-, tri-, and tetra-nanofluids at the lowest and highest heat loads tested, respectively. At the lowest heat load of 136.4 W, every nanofluid reported an enhancement value over pure water in terms of the Nusselt number and heat transfer coefficient; however, not every nanofluid recorded a hydrothermal performance value greater than unity, which represents the performance of the base fluid.

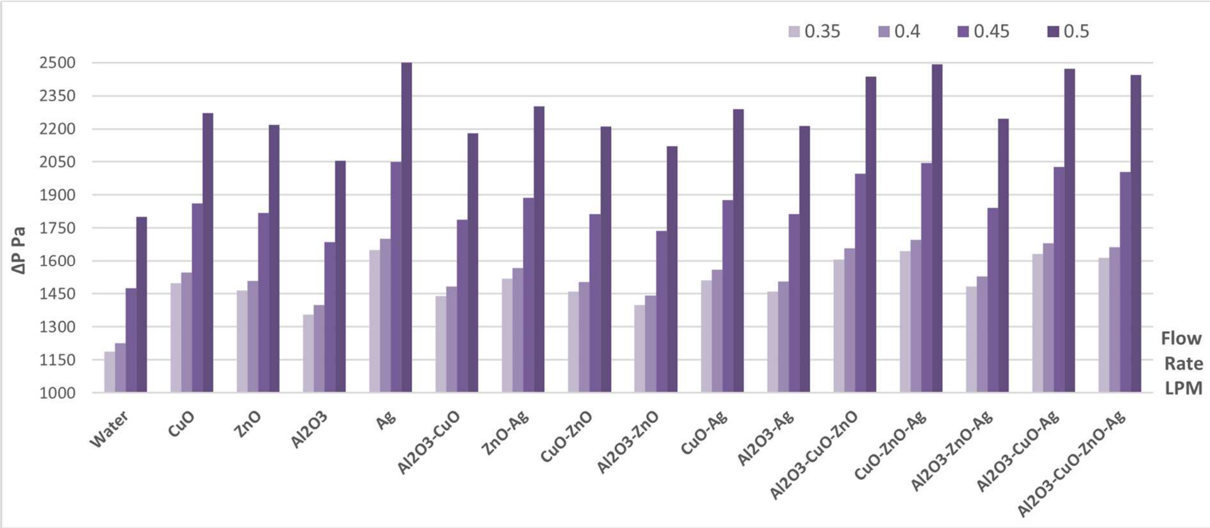

Fig. 23. Fluctuation in pressure difference versus nanofluid coolant types at different flow rates and φ = 0.025% concentration per volume.

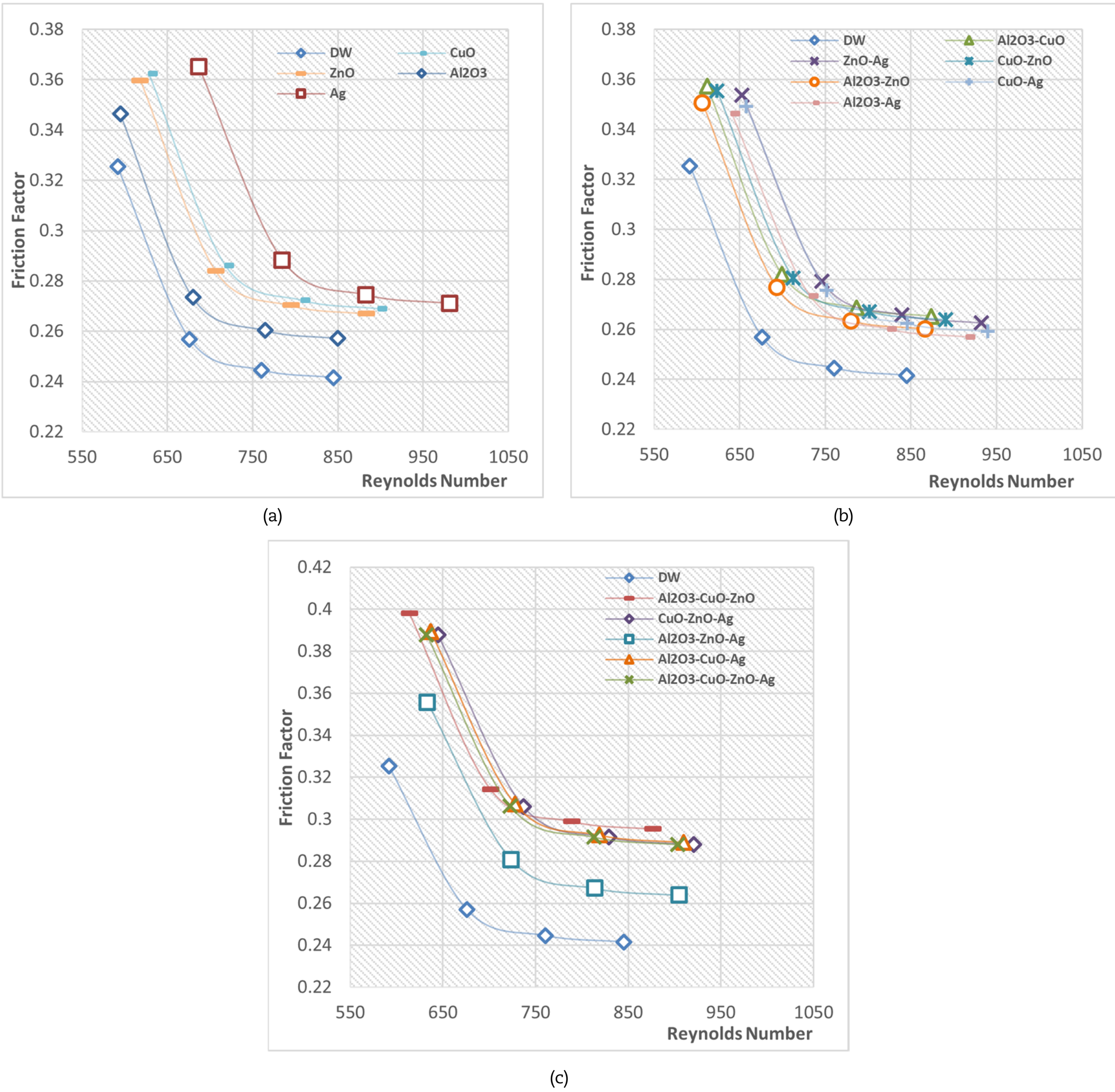

Fig. 24. Friction factor versus Reynolds number at φ = 0.025% per volume, (a) mono-nanofluids, (b) di-nanofluids, (c) tri and tetra-nanofluids.

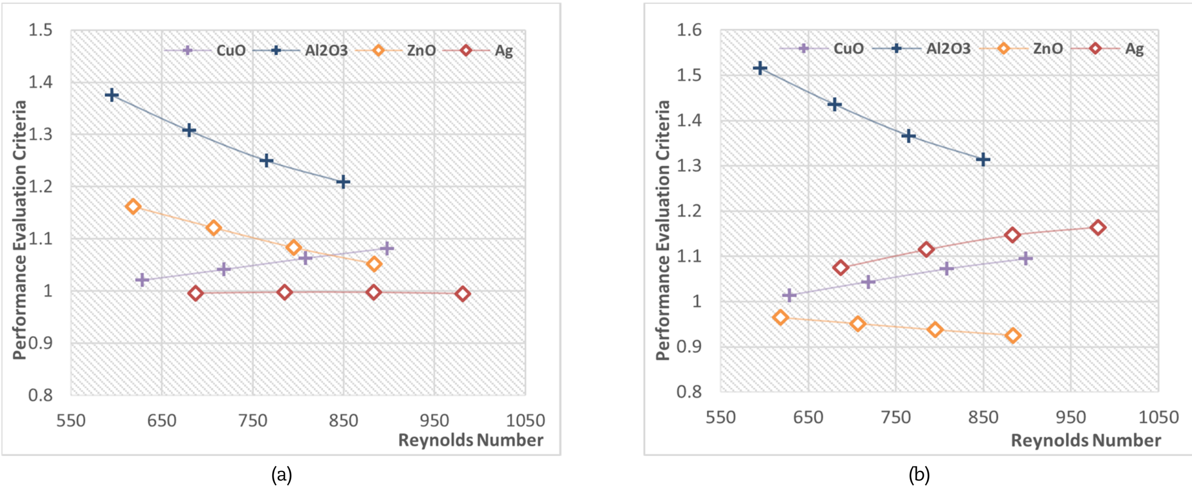

Fig. 25. Performance evaluation criteria at φ = 0.025% per volume for mono-nanofluids, (a) heat load 136.4 W, (b) heat load 194.4 W.

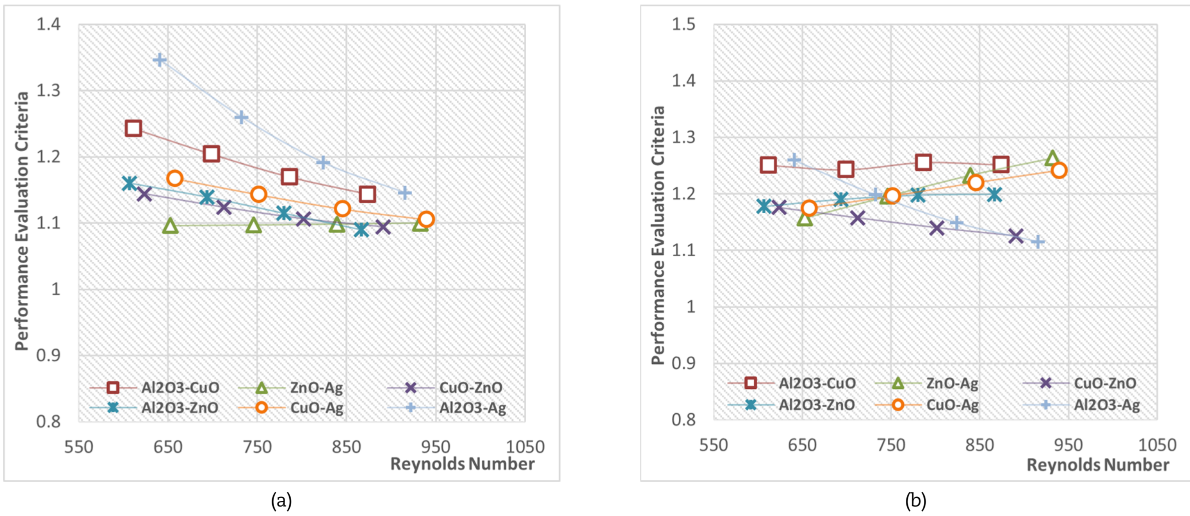

Fig. 26. Performance evaluation criteria at φ = 0.025% per volume for di-nanofluids, (a) heat load 136.4 W, (b) heat load 194.4 W.

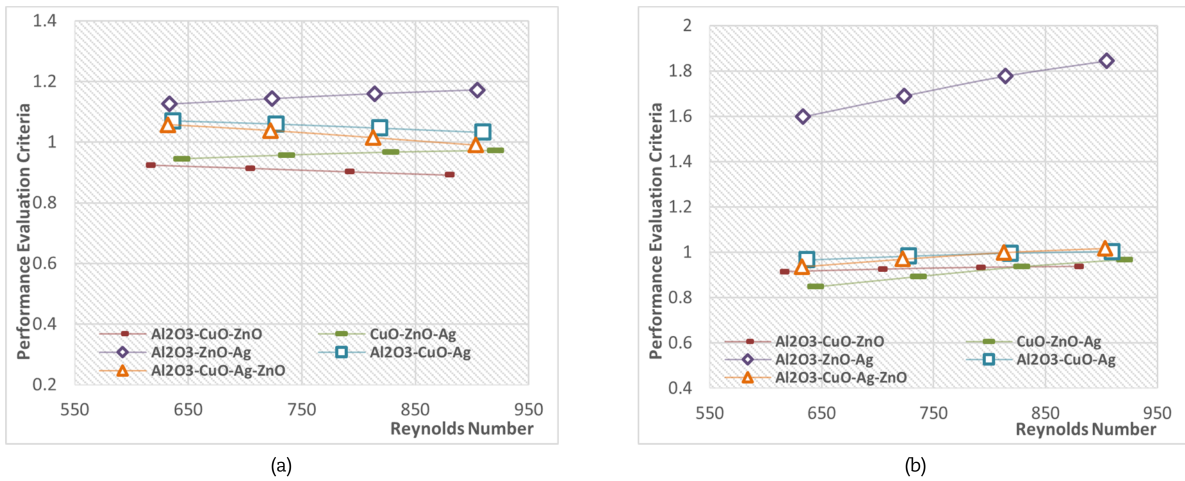

Fig. 27. Performance evaluation criteria at φ = 0.025% per volume for tri and tetra-nanofluids, (a) heat load 136.4 W, (b) heat load 194.4 W.

Moreover, all nanofluids demonstrated performance greater than unity, as demonstrated in of Figs. 25(a), 26(a), and 27(a), except for CuO–ZnO–Ag, and Al_2O_3–CuO–ZnO tri-nanofluids, which were distinguished by a higher friction factor. Additionally, it can be seen from Figs. 25(a), 26(a), and 27(a), that at the lowest heat load of 136.4 W, certain types of nanofluids such as ZnO and Al_2O_3 mono nanofluids performed better as the Reynolds number increased, whereas other types exhibited the opposite behavior. However, at the di level of hybridization as shown in Fig. 26(a), all of them showed a decreasing trend in performance with increasing Reynolds number values except ZnO-Ag, which showed a constant performance, while at the tri and tetra levels of hybridization, as shown in Fig. 27(a), all types showed approximately constant performance with manipulating Reynolds number; however, tri ZnO-Ag hybridizations showed a slightly increasing trend.

Table 7. Maximum and minimum values of enhancements recorded for all trials in all operating conditions φ = 0.025% per volume.

	Flow Parameters		HTC%		Nu%		PEC	
High heat load 194.4 W	High Velocity 0.5 LPM	Maximum Value	Al_2O_3- ZnO-Ag	1.168	Al_2O_3- ZnO-Ag	1.015	Al_2O_3-ZnO-Ag	1.845
		Minimum Value	ZnO	0.096	ZnO	0.023	ZnO	0.925
	Low Velocity 0.35 LPM	Maximum Value	Al_2O_3-ZnO-Ag	0.879	Al_2O_3-ZnO-Ag	0.746	Al_2O_3-ZnO-Ag	1.598
		Minimum Value	CuO-ZnO-Ag	0.086	CuO-ZnO-Ag	0.010	CuO-ZnO-Ag	0.847
Low heat load 136.4 W	High Velocity 0.5 LPM	Maximum Value	Al_2O_3	0.381	Al_2O_3	0.287	Al_2O_3	1.209
		Minimum Value	Al_2O_3-CuO-ZnO	0.170	Al_2O_3-CuO-ZnO	0.090	Al_2O_3-CuO-ZnO	0.892
	Low Velocity 0.35 LPM	Maximum Value	Al_2O_3	0.572	Al_2O_3	0.465	Al_2O_3	1.375
		Minimum Value	Ag	0.203	Ag	0.118	Al_2O_3-CuO-ZnO	0.924

Furthermore, at the highest heat load of 194.4 W, despite reporting an enhancement value in terms of Nusselt number and heat transfer coefficient over pure water, not all of them recorded a higher value than unity in terms of hydrothermal performance as well. In addition, as of Figs. 25(b), 26(b), and 27(b) shows, all mono- and di-nanofluids performed better than unity, except for ZnO mono-nanofluid; all tri- and tetra-nanofluids performed closer to or slightly worse than unity, except for Al_2O_3-ZnO-Ag, which performed better than the unity value and had the best overall performance over the tested parameters. Furthermore, as can be seen in of Figs. 25(b), 26(b), and 27(b), not all nanofluids demonstrated an increasing trend in terms of hydrothermal performance by increasing Reynolds number, even at the lowest heat flux and at the maximum heat load of 194.4 W. Except for the hydrothermal performance of Ag mono-nanofluid, which changed from constant performance to an increasing trend with Reynolds number, CuO, Al_2O_3, and ZnO mono-nanofluids all exhibited the same trend with increasing Reynolds number; at the maximum heat load, ZnO, however, recorded a value less than unity. Furthermore, at the di level of hybridization, as illustrated in Fig. 26(b), in contrast to the lowest heat flux, certain di hybrid nanofluid types, such as ZnO-Ag and CuO-Ag, demonstrated an increasing trend with increasing Reynolds number, whereas other types, such as Al_2O_3-Ag and CuO-ZnO, demonstrated the opposite, and the remaining types demonstrated approximately constant performance. Furthermore, as illustrated in Fig. 27(b), at the tri and tetra stages of hybridization, all types demonstrated nearly constant performance when Reynolds numbers were changed, except for Al_2O_3-ZnO-Ag, which not only recorded the best overall performance of the tested coolants but also displayed an increasing trend in performance with rising Reynolds numbers.

In summary, Table 7 shows that, out of all the tested nanofluids, Al_2O_3-ZnO-Ag exhibited the maximum heat transfer coefficient, Nusselt number ratios, and performance evaluation criteria at the highest heat flux of 194.4 watts and φ = 0.025% per volume. However, among all tested nanofluids, Al_2O_3 mono nanofluid demonstrated the highest values for HTC%, Nu%, and PEC at the lowest heat flux of 136.4 watts.

Finally, even though all nanofluids showed a higher heat transfer coefficient, their performance depends on multiple factors besides the heat transfer coefficient. Furthermore, it can be observed that Al_2O_3 exhibits a different behavior in terms of Nusselt variation with Reynolds number when hybridized with ZnO and Ag. All nanofluids demonstrated an improvement with increasing heat load in terms of heat transfer coefficient and Nusselt number, but the percentage of improvement relative to pure base fluid was not consistent. A higher heat load improved the performance of Al_2O_3, ZnO-Ag, CuO-Ag, and Al_2O_3-ZnO-Ag, whereas ZnO, Ag, Al_2O_3-Ag, and the majority of tri and tetra nanofluids exhibited the opposite behavior. Additionally, at the maximum heat flux of 194.4 watts, ZnO mono nanofluid and CuO-ZnO-Ag tri nanofluid performed the worst overall at the highest and lowest flow velocities, respectively. While at the lowest heat flux of 136.4 watts, Al_2O_3-CuO-ZnO tri nanofluid recorded the lowest HTC%, Nu%, and PEC. However, Ag mono nanofluid showed the worst values of HTC% and Nu% at the same heat flux but for a lower velocity value of 0.35 LPM.

4. Conclusions and Recommendations

The nature of each particle has a unique function in improving the fluid's overall hydrothermal performance. Understanding how adding nanoparticles might improve the thermophysical properties and heat transfer characteristics of base fluids, as well as how to architecturally design a nanofluid with various types of nanoparticles to approach the ideal nanofluid for thermal applications, is crucial and will have a significant impact on many industries. In conclusion, for the current investigation:

- All varieties of nanofluids demonstrated positive enhancement values for the Nusselt number ratio and heat transfer coefficient ratio at 0.025% micro-concentration, despite variations in their enhancement levels.
- The maximum recorded PEC for all tested parameters was 1.845 at the highest heat flux and highest flow velocity by Al_2O_3-ZnO-Ag tri nanofluid, however, maximum enhancement values of Nusselt number and PEC are not an exclusive thing for higher levels of hybrid nanofluids, as Al_2O_3 mono nanofluid recorded the highest enhancement value over all tested nanofluids at the lowest heat load tested.
- The minimum recorded PEC was 0.847 at the highest heat flux and lowest flow velocity by CuO-ZnO-Ag tri hybrid nanofluid, which is lower than unity. ZnO, Al_2O_3-CuO-ZnO, and CuO-ZnO-Ag are the only types that showed a PEC value lower than unity; however, those values were not tested in all operating conditions.
- Upon increasing the micro-concentration from 0.025% to 0.05% per volume, all varieties of mono nanofluids demonstrated an increase in Nusselt number and heat transfer coefficient enhancement levels; in contrast, hybrid nanofluids exhibited the opposite reaction, with the Nusselt number ratio decreasing even further below the base fluid values as the concentration increased and the heat transfer coefficient declining as well.
- At higher heat load all nanofluids showed a higher heat transfer coefficient, Nusselt number, and PEC.
- Increasing the heat load magnifies the enhancement ability by increasing the flow rate.
- In addition to choosing lower-density nanoparticles, a more homogeneous molecular crystal structure of the nanoparticles relative to the base fluid may facilitate heat transfer through micro-convection.
- Particularly at higher Reynolds numbers, nanoparticles with a relatively higher density and larger particle size increase the probability of collisions, which increases the particle momentum magnitude, thus enhancing heat transfer in nanofluids.

- The higher enhancement value of Al_2O_3-ZnO-Ag compared to other tri-nanofluids may be due in part to the Soret phenomenon and Dufur effect, as the particles in this blend have different sizes, shapes, and overall densities, allowing the hybrid nanofluid to benefit from each component in its blend.
- At higher concentrations, hybrid nanoparticles may form relatively larger hybrid clusters that block one another from passing through the microchannel gaps, increasing the microchannel's thermal resistance. On the other hand, hybrid nanoparticles can penetrate through microchannels when a smaller cluster network is created by employing a lower micro-concentration level. This enhances the overall heat transfer capabilities by decreasing thermal resistance.

From a future perspective, more research on hybrid nanofluids needs to be conducted. To evaluate how nanoparticle agglomeration affects the size and number of crystals in hybrid nanofluids, testing and observation are required. The literature currently lacks higher hybridization levels for materials based on organic matter and graphene. Moreover, studies on the hybridization ratio effect, other geometric characteristics of microchannels, like unique patterns and bionic configurations, and higher hybridization levels for hybrid nanofluids are promising.

Author Contributions

M. Salah Elsherbiny planned and initiated the project, suggested and conducted the experiments, and analyzed the empirical results. M. Ali, M. Shahin and M. El-Kady provided supervision and guidance and examined the theory validation. The manuscript was written with the contributions of all authors. All authors discussed the results, reviewed, and approved the final version of the manuscript.

Acknowledgments

We would like to express our sincere gratitude to British University in Egypt and Al Azhar University for their invaluable support and resources in facilitating this research.

Conflict of Interest

The authors declared no potential conflicts of interest concerning the research, authorship, and publication of this article.

Funding

The authors received no financial support for the research, authorship, and publication of this article.

Data Availability Statements

The datasets generated and/or analyzed during the current study are available from the corresponding author upon reasonable request.

Nomenclature

Notation		sp	Specimen
h	Heat transfer coefficient	np	Nanoparticles
f	Friction factor	c	Coolant
T	Temperature	bf	Base fluid
k	Thermal conductivity	nf	Nanofluid
C_p	Specific heat capacity	in	Inlet
A	Area	out	Outlet
Q	Heat transfer	m	Mean
L	Length	n	Number
H	Height	t	Total
w	Width	r	Ratio
d	Diameter	•	Rated
x	Spacing, distance	***Greek symbols***	
Å	Angstrom	ρ	Density
W	Uncertainty of dependent variable	μ	Dynamic viscosity
V	Volume	φ	Nanoparticle's volume fraction %
m	Mass	Δ	Difference
R	The function of the independent variable	Ω	Pumping power
X	Independent variable	***Abbreviation description***	
v	Velocity	SDS	Sodium dodecyl sulfate
p	Pressure	LPM	Liter per min
l	Characteristic length	CPU	Central processing unit

Chemical formula		Gr	Graphene
Al_2O_3	Aluminum oxide	MEMS	Micro-electro-mechanical systems
CuO	Copper oxide	MCHS	Microchannel heat sink
ZnO	Zinc oxide	TEM	Transmission electron microscopy
Ag	Silver	SAED	Selective area electron diffraction
TiO_2	Titanium oxide	DAQ	Data acquisition
SiO_2	Silicon oxide	CMC	Carboxymethyl cellulose
Cu	Copper	PCM	Phase change material
Zn	Zinc	FEM	Finite element method
MgO	Methylglyoxal	MWCNT	Multi-walled carbon nanotube
Subscript and superscript		CFD	Computational fluid dynamics
S	Surface	RMC	Recharging microchannels
Ch	Channel	HTC	Heat transfer coefficient
f	Fin	PEC	Performance evaluation criteria
Cr	Cross-sectional	HYNF	Hybrid nanofluid
h	Hydraulic	***Dimensionless description***	
b	Base	Nu	Nusselt number
u	Unit	Re	Reynold number
e	Electric		

References

[1] Vajravel, L.V., et al., Experimental investigations on heat transfer in a new minichannel heat sink, *International Journal of Thermal Sciences*, 140, 2019, 144-153.
[2] Tuckerman, D.B., Pease, R.F.W., High-performance heat sinking for VLSI, *IEEE Electron Device Letters*, 2(5), 1981, 126-129.
[3] Khan, A., et al., Review of micro and mini channels, porous heat sinks with hydrophobic surfaces for single phase fluid flow, *Journal of the Taiwan Institute of Chemical Engineers*, 132, 2022, 104186.
[4] Japar, W.M.A.A., et al., A review of passive methods in microchannel heat sink application through advanced geometric structure and nanofluids: Current advancements and challenges, *Nanotechnology Reviews*, 9(1), 2020, 1192-1216.
[5] Choi, S.U., Eastman, J.A., *Enhancing thermal conductivity of fluids with nanoparticles*, Argonne National Lab. (ANL), Argonne, IL (United States), 1995.
[6] Suresh, S., et al., Effect of Al2O3–Cu/water hybrid nanofluid in heat transfer, *Experimental Thermal and Fluid Science*, 38, 2012, 54-60.
[7] Ramadhan, A., Azmi, W., Mamat, R., Heat transfer characteristics of car radiator using tri-hybrid nanocoolant, *IOP Conference Series: Materials Science and Engineering*, IOP Publishing, 2020.
[8] Ali, A.R.I., Salam, B., A review on nanofluid: preparation, stability, thermophysical properties, heat transfer characteristics and application, *SN Applied Sciences*, 2(10), 2020, 1636.
[9] Vinoth, R., Sachuthananthan, B., Flow and heat transfer behavior of hybrid nanofluid through microchannel with two different channels, *International Communications in Heat and Mass Transfer*, 123, 2021, 105194.
[10] Nitiapiruk, P., et al., Performance characteristics of a microchannel heat sink using TiO2/water nanofluid and different thermophysical models, *International Communications in Heat and Mass Transfer*, 47, 2013, 98-104.
[11] Kumar, V., et al., Thermal and thermo-hydraulic behaviour of alumina-graphene hybrid nanofluid in minichannel heat sink: An experimental study, *International Journal of Energy Research*, 45(15), 2021, 20700-20714.
[12] Sriharan, G., Harikrishnan, S., Ali, H.M., Enhanced heat transfer characteristics of the mini hexagonal tube heat sink using hybrid nanofluids, *Nanotechnology*, 33(47), 2022, 475403.
[13] Ataei, M., et al., Heat transfer and flow characteristics of hybrid Al2O3/TiO2–water nanofluid in a minichannel heat sink, *Heat and Mass Transfer*, 56, 2020, 2757-2767.
[14] Ma, H., et al., Numerical investigation on heat transfer behavior of thermally developing flow inside rectangular microchannels, *Case Studies in Thermal Engineering*, 24, 2021, 100856.
[15] Elbadawy, I., Fayed, M., Reliability of Al2O3 nanofluid concentration on the heat transfer augmentation and resizing for single and double stack microchannels, *Alexandria Engineering Journal*, 59(3), 2020, 1771-1785.
[16] Al-Rashed, A.A., et al., Numerical investigation of non-Newtonian water-CMC/CuO nanofluid flow in an offset strip-fin microchannel heat sink: thermal performance and thermodynamic considerations, *Applied Thermal Engineering*, 155, 2019, 247-258.
[17] Singh, S.K., et al., Augmentation of heat transfer in a microtube and a wavy microchannel using hybrid nanofluid: A numerical investigation, *Mathematical Methods in the Applied Sciences*, 2020, https://doi.org/10.1002/mma.6849.
[18] Samal, S.K., Moharana, M.K., Thermo-hydraulic and entropy generation analysis of recharging microchannel using water-based graphene–silver hybrid nanofluid, *Journal of Thermal Analysis and Calorimetry*, 143(6), 2021, 4131-4148.
[19] Jajja, S.A., et al., Water cooled minichannel heat sinks for microprocessor cooling: Effect of fin spacing, *Applied Thermal Engineering*, 64(1-2), 2014, 76-82.
[20] Khoshvaght-Aliabadi, M., Arani, Z., Rahimpour, F., Influence of Al2O3–H2O nanofluid on performance of twisted minichannels, *Advanced Powder Technology*, 27(4), 2016, 1514-1525.
[21] Yan, Y., et al., Thermal-hydraulic performance enhancement of miniature heat sinks using connected Y-shaped fractal micro-channels, *Chemical Engineering and Processing-Process Intensification*, 166, 2021, 108487.
[22] El-Khouly, M., El Bouz, M., Sultan, G., Experimental and computational study of using nanofluid for thermal management of electronic chips, *Journal of Energy Storage*, 39, 2021, 102630.
[23] Azizi, Z., Alamdari, A., Malayeri, M., Convective heat transfer of Cu–water nanofluid in a cylindrical microchannel heat sink, *Energy Conversion and Management*, 101, 2015, 515-524.
[24] Kumar, V., Sarkar, J., Yan, W.-M., Thermal-hydraulic behavior of lotus like structured rGO-ZnO composite dispersed hybrid nanofluid in mini channel heat sink, *International Journal of Thermal Sciences*, 164, 2021, 106886.
[25] Bahiraei, M., Jamshidmofid, M., Goodarzi, M., Efficacy of a hybrid nanofluid in a new microchannel heat sink equipped with both secondary channels and ribs, *Journal of Molecular Liquids*, 273, 2019, 88-98.
[26] Sarvar-Ardeh, S., Rafee, R., Rashidi, S., Hybrid nanofluids with temperature-dependent properties for use in double-layered microchannel heat sink; hydrothermal investigation, *Journal of the Taiwan Institute of Chemical Engineers*, 124, 2021, 53-62.

[27] Souby, M.M., Bargal, M.H., Wang, Y., Thermohydraulic performance improvement and entropy generation characteristics of a microchannel heat sink cooled with new hybrid nanofluids containing ternary/binary hybrid nanocomposites, *Energy Science & Engineering*, 9(12), 2021, 2493-2513.
[28] Zahan, I., Nasrin, R., Khatun, S., Thermal performance of ternary-hybrid nanofluids through a convergent-divergent nozzle using distilled water-ethylene glycol mixtures, *International Communications in Heat and Mass Transfer*, 137, 2022, 106254.
[29] Ho, C., et al., Cooling performance of mini-channel heat sink with water-based nano-PCM emulsion-An experimental study, *International Journal of Thermal Sciences*, 164, 2021, 106903.
[30] Selimefendigil, F., Öztop, H.F., Analysis of hybrid nanofluid and surface corrugation in the laminar convective flow through an encapsulated PCM filled vertical cylinder and POD-based modeling, *International Journal of Heat and Mass Transfer*, 178, 2021, 121623.
[31] Barnoon, P., Numerical assessment of heat transfer and mixing quality of a hybrid nanofluid in a microchannel equipped with a dual mixer, *International Journal of Thermofluids*, 12, 2021, 100111.
[32] Pordanjani, A.H., et al., Effect of magnetic field on mixed convection and entropy generation of hybrid nanofluid in an inclined enclosure: sensitivity analysis and optimization, *The European Physical Journal Plus*, 134, 2019, 1-20.
[33] Izadi, M., et al., Coupled FHD–MHD free convection of a hybrid nanoliquid in an inversed T-shaped enclosure occupied by partitioned porous media, *Numerical Heat Transfer, Part A: Applications*, 76(6), 2019, 479-498.
[34] Rajarathinam, M., Nithyadevi, N., Chamkha, A.J., Heat transfer enhancement of mixed convection in an inclined porous cavity using Cu-water nanofluid, *Advanced Powder Technology*, 29(3), 2018, 590-605.
[35] Bazkhane, S., Zahmatkesh, I., Taguchi–based sensitivity analysis of hydrodynamics and heat transfer of nanofluids in a microchannel heat sink (MCHS) having porous substrates, *International Communications in Heat and Mass Transfer*, 118, 2020, 104885.
[36] Farsad, E., et al., Numerical simulation of heat transfer in a micro channel heat sinks using nanofluids, *Heat and Mass Transfer*, 47(4), 2011, 479-490.
[37] Krishna, V.M., et al., Numerical investigation of heat transfer and pressure drop for cooling of microchannel heat sink using MWCNT-CuO-Water hybrid nanofluid with different mixture ratio, *Materials Today: Proceedings*, 42, 2021, 969-974.
[38] Mohammed, H., Gunnasegaran, P., Shuaib, N., Heat transfer in rectangular microchannels heat sink using nanofluids, *International Communications in Heat and Mass Transfer*, 37(10), 2010, 1496-1503.
[39] Hung, T.-C., et al., Heat transfer enhancement in microchannel heat sinks using nanofluids, *International Journal of Heat and Mass Transfer*, 55(9-10), 2012, 2559-2570.
[40] Bahiraei, M., Heshmatian, S., Thermal performance and second law characteristics of two new microchannel heat sinks operated with hybrid nanofluid containing graphene–silver nanoparticles, *Energy Conversion and Management*, 168, 2018, 357-370.
[41] Singh, B., et al. Experimental and numerical analysis of micro-scale heat transfer using carbon based nanofluid in microchannel for enhanced thermal performance, *IOP Conference Series: Materials Science and Engineering*, IOP Publishing, 2016.
[42] Kumar, V., Sarkar, J., Numerical and experimental investigations on heat transfer and pressure drop characteristics of Al2O3-TiO2 hybrid nanofluid in minichannel heat sink with different mixture ratio, *Powder Technology*, 345, 2019, 717-727.
[43] Aglawe, K., Yadav, R., Thool, S., Preparation, applications and challenges of nanofluids in electronic cooling: A systematic review, *Materials Today: Proceedings*, 43, 2021, 366-372.
[44] Chandravadhana, A., NandaKumar, V., Venkatramanan, K., Mono and hybrid nanofluid based heat sink technologies-a review, *Journal of Physics: Conference Series*, IOP Publishing, 2020.
[45] Duangthongsuk, W., Wongwises, S., An experimental investigation on the heat transfer and pressure drop characteristics of nanofluid flowing in microchannel heat sink with multiple zigzag flow channel structures, *Experimental Thermal and Fluid Science*, 87, 2017, 30-39.
[46] Kandlikar, S.G., High flux heat removal with microchannels—a roadmap of challenges and opportunities, *Heat Transfer Engineering*, 26(8), 2005, 5-14.
[47] Vasilev, M., Abiev, R.S., Kumar, R., Effect of microchannel heat sink configuration on the thermal performance and pumping power, *International Journal of Heat and Mass Transfer*, 141, 2019, 845-854.

ORCID ID

M. Salah Elsherbiny https://orcid.org/0009-0008-2555-8744
Moatsem Shahin https://orcid.org/0000-0003-3662-2453

How to cite this article: Elsherbiny M.S., Ali M., Shahin M., El-Kady M. Experimental Study on the Effect of Micro Concentrations of Hybrid Nanofluids through Microchannel Heat Sinks, *J. Appl. Comput. Mech.*, 11(2), 2025, 303-326. https://doi.org/10.22055/jacm.2024.46291.4494